https://doi.org/10.5194/egusphere-2026-3341
Preprint. Discussion started: 9 July 2026

Adaptive Observation Weighting in TCKF1D-Var for Ground-Based Multi-Sensor Thermodynamic Retrievals Prior to Nocturnal Heavy Precipitation over China

Qi Zhang[1,3], Tianmeng Chen[2,4], and Jianping Guo[2,4]

[1]Key Open Laboratory of Intelligent Meteorological Observation Technology, China Meteorological Administration, Beijing 100081, China
[2]State Key Laboratory of Severe Weather Meteorological Science and Technology & Specialized Meteorological Support Technology Research Center, Chinese Academy of Meteorological Sciences, Beijing 100081, China
[3]Engineering Technology Research and Development Center, China Huayun Meteorological Technology Group Co. Ltd., Beijing 100081, China
[4]Field Scientific Experiment Base for Low-Altitude Economy Meteorological Support of Unmanned Aviation in Guangdong–Hong Kong–Macao Greater Bay Area, China Meteorological Administration, Shenzhen 518108, China

Correspondence to: Jianping Guo (jpguo@cma.gov.cn) and Tianmeng Chen (chentm@cma.gov.cn)

Abstract. Ground-based microwave radiometers (GMWRs) and Mie–Raman lidars (MRLs) provide valuable thermodynamic observations for atmospheric profiling, but conventional variational retrieval frameworks typically rely on static observation weighting assumptions that may not adequately represent varying observation quality under precipitation conditions. To address this limitation, an adaptive observation weighting framework based on the Thermodynamic-Constrained Kalman Filter 1D-Var framework (TCKF1D-Var) is developed and evaluated using 107 nocturnal heavy-precipitation cases. The proposed method dynamically estimates observational contributions during the retrieval process and is applied to GMWR, MRL, and GMWR–MRL synergistic retrievals. Retrieval performance is assessed against radiosonde observations and compared with that of a conventional static-weighting TCKF1D-Var framework. Results show that the adaptive weighting approach consistently improves retrieval accuracy, with the largest benefits found for water vapor mass mixing ratio profiles. For both GMWR and MRL retrievals, reductions in mean bias and root-mean-square error are obtained relative to the static-weighting framework. The synergistic retrieval further improves moisture-profile retrievals and generally achieves the best overall performance among all experiments. Diagnostic analyses reveal that the adaptive framework dynamically adjusts the utilization of observational information according to sensor characteristics and atmospheric conditions, while redistributing observational influence between GMWR and MRL measurements during synergistic retrievals. These results demonstrate that adaptive observation weighting provides an effective strategy for improving thermodynamic profile retrievals under heavy-precipitation pre-onset conditions.

1 Introduction

Nocturnal heavy precipitation (NHP) events pose a substantial threat to society because they frequently occur during periods of reduced public awareness and emergency response capacity, thereby increasing the risk of casualties and economic losses. Recent studies (Luo et al., 2020; Chen et al., 2021; Richardson et al., 2024; Sun et al., 2025; Gao et al., 2026) have further indicated that both the frequency and intensity of NHP events have increased over many regions of China under a warming climate. Improving the lead time and accuracy of NHP forecasts has therefore become an important objective for both operational forecasting and atmospheric research. Achieving this objective requires a more accurate characterization of the atmospheric conditions that govern the initiation and subsequent evolution of heavy precipitation (Löhnert et al., 2026). In particular, the initiation and rapid intensification of convective precipitation are strongly controlled by the pre-onset thermodynamic environment, especially the vertical distributions of temperature and water vapor (Behrendt et al., 2011; Wulfmeyer et al., 2011; Kirshbaum et al., 2018; Ahmed et al., 2020). Consequently, the growing deployment of ground-based atmospheric profiling instruments has created new opportunities for extending the prediction lead time of heavy precipitation through the monitoring of atmospheric thermodynamic structures before precipitation onset.

Among these instruments, ground-based microwave radiometers (GMWRs) have become widely used owing to their capability to continuously observe atmospheric thermal and moisture conditions under nearly all weather conditions (Güldner and Spänkuch, 2001; Löhnert and Maier, 2012; Cimini et al., 2015; Temimi et al., 2020). By measuring naturally emitted microwave radiation from atmospheric gases and cloud liquid water at multiple frequencies, GMWRs provide continuous retrievals of temperature and humidity profiles throughout the troposphere, with typical retrieval products achieving temporal resolutions of approximately 2 minutes and vertical resolutions ranging from less than 100 meters within the planetary boundary layer to several hundred meters in the free troposphere (Askne and Westwater, 1986; Hewison, 2007; Yan et al., 2020). In contrast to the passive observing strategy employed by GMWRs, Mie-Raman Lidars (MRLs) actively probe the atmosphere using laser backscatter techniques. A MRL operating at a wavelength of 354.7 nm simultaneously detects nitrogen Raman signals near 386.7 nm and water-vapor Raman signals near 407.5 nm, enabling high-resolution profiling of atmospheric moisture (Vaughan et al., 1988; Di Girolamo et al., 2017; Lange et al., 2019 and 2025; Whiteman et al., 2010; Wulfmeyer et al., 2015a; Behrendt et al., 2002). Compared with GMWRs, MRLs provide substantially finer and nearly height-independent vertical resolution, typically better than 45 meters, allowing detailed characterization of moisture gradients, turbulent mixing processes, and boundary-layer structures that are often closely related to convection initiation (Wulfmeyer et al., 2011; Gambacorta et al., 2025). However, Raman lidar observations are strongly affected by cloud attenuation, precipitation, and aerosol loading, which limits their capability for continuous all-weather monitoring (Wandinger, 2005; Filioglou et al., 2017). Given the complementary strengths and limitations of these two observing systems, considerable effort has been devoted to combining microwave radiometer and Raman lidar observations for thermodynamic profile retrievals and has demonstrated that synergistic retrieval frameworks can significantly improve the

https://doi.org/10.5194/egusphere-2026-3341
Preprint. Discussion started: 9 July 2026

accuracy and vertical resolution of atmospheric temperature and humidity profiles while extending the observational coverage from the planetary boundary layer into the free troposphere (Löhnert et al., 2004; Ji et al., 2025; Barrera-Verdejo et al., 2016; Meunier et al., 2015; Foth et al., 2015; Gerber et al., 2004; Han et al., 1994).

Despite these advances, an important limitation remains. Most existing retrieval systems primarily focus on improving retrieval accuracy, whereas relatively little attention has been paid to quantifying the individual contributions of different observations to the final retrieval solution. For microwave radiometers, methods capable of diagnosing the contribution of individual observation channels remain limited. For Raman lidar retrievals, the relative importance of measurements acquired at different range bins has rarely been systematically investigated. Furthermore, within multi-sensor retrieval frameworks, few studies have attempted to quantify how observations from different instruments contribute to the retrieved thermodynamic profiles or how these contributions vary with height and atmospheric conditions. This lack of diagnostic capability restricts the physical interpretation of retrieval results and limits our understanding of the information content provided by different observing systems. To address these challenges, this study extends the Thermodynamic Constrained Kalman Filter One-Dimensional Variational (TCKF1D-Var) retrieval framework developed in our previous work (Zhang et al., 2026a and 2026b) by introducing an adaptive observation weighting scheme into the retrieval cost function. Unlike conventional approaches that rely on fixed observation weights, the proposed framework incorporates dynamically optimized weighting coefficients that are estimated during the retrieval process. The resulting methodology provides a quantitative measure of the relative contribution of individual observations to the retrieved thermodynamic profiles. Consequently, it enables a systematic assessment of the information content associated with GMWR channels, MRL range bins, and observations from the two instruments within a synergistic retrieval configuration.

The remainder of this paper is organized as follows. Section 2 describes the observational instruments and datasets used in this study. Section 3 introduces the methodological developments of the TCKF1D-Var framework, including the implementation of the adaptive observation weighting scheme. Section 4 evaluates the retrieval performance and analyzes the contributions of individual observations in the GMWR, MRL, and GMWR-MRL synergistic retrieval experiments. Finally, Section 5 summarizes the main findings and discusses future applications of the proposed methodology.

2 Instrument and data

As part of the modernization of the national atmospheric observing network, the China Meteorological Administration began deploying GMWRs and MRLs at key observational sites in 2021 (Zhang et al., 2025; Shao et al., 2025). This initiative has substantially enhanced the capability for continuous profiling of atmospheric thermodynamic and dynamic structures. By the end of 2025, MRL systems had been deployed at 56 radiosonde stations participating in the international upper-air data exchange program, with each site providing more than one year of operational observations (Figure 1). The observational datasets used in this study consist of GMWR measurements, MRL observations, radiosonde soundings, and surface precipitation records. Detailed technical specifications for these datasets are described in Section 2.1, Section 2.2, and Section 2.3, respectively. In addition, the atmospheric prior profiles used to initialize the retrieval framework are introduced in Section 2.4.

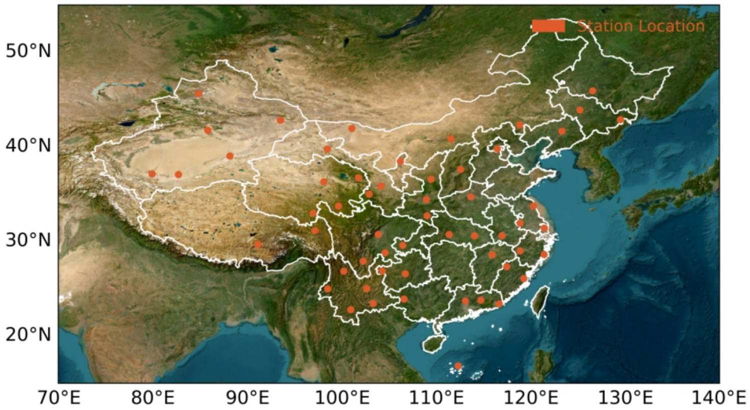

Figure 1. Geographic distribution of the co-located radiosonde, GMWR, and MRL observation sites used in this study across China. The topographic basemap was obtained from ArcGIS Online and is provided by Esri | Powered by Esri (Esri et al., 2025).

2.1 GMWR

Compared with our previous study (Zhang et al., 2026a), the number of GMWR channels used in the present work has been reduced from 14 to 9. This adjustment was made to ensure the consistency and comparability of observations across the nationwide dataset. Specifically, the 56 observational sites included in this study are equipped with 7 different models of ground-based microwave radiometers, each with slightly different channel configurations. To establish a uniform observation vector applicable to all stations, only the channels common to all instrument models were retained. As a result, the retrieval framework utilizes measurements at 22.235, 23.035, 23.835, 26.235, 51.25, 52.28, 53.85, 54.94, and 56.66 GHz. Although this channel selection reduces the total number of available observations relative to Zhang et al. (2026a), it ensures methodological consistency and enables the retrieval framework to be applied uniformly across the entire observational network.

2.2 MRL

The MRLs emits laser pulses at 354.7, 532.1, and 1064.1 nm with single-pulse energies of 0.6, 1.5, and 1.8 mJ, respectively, and a repetition rate of 1000 Hz. Beam divergence is 0.3 mrad for the ultraviolet and green channels and 0.5 mrad for the infrared channel. A Cassegrain telescope with a 30 cm primary mirror and a field of view of 1 mrad collects the backscattered signals. The receiver includes eight detection channels, three of which are Raman channels centered at 386.7, 407.5, and 607.6 nm for retrieving atmospheric water vapor and nitrogen signals. These channels are equipped with narrowband interference filters (bandwidth 0.5–1 nm) with high peak transmission (80–90%) and strong out-of-band rejection (OD6–OD7). Photomultiplier tube (PMT) detectors with 40% quantum efficiency, a dark count rate of 100 counts/s, and a maximum linear count rate of 1.5×10^6 counts/s are used. The system achieves a pulse-pair resolution of 30 ns, an effective vertical resolution of 30 m, and a blind range height of 150 m. Detailed system specifications are summarized in Zhang et al. (2026b).

2.3 In-situ observations

At the co-located radiosonde stations, routine soundings were conducted twice daily, at approximately 00:00 and 12:00 UTC. The radiosonde measurements provide temperature with a resolution of 0.1 K and an accuracy of 0.5 K, relative humidity with a resolution of 1% and an accuracy of 5%, and pressure with a resolution of 0.1 hPa and an accuracy of 0.5 hPa (Cao et al., 2026). These observations serve as independent reference data for evaluating the accuracy of retrieved thermodynamic profiles. In addition, hourly accumulated precipitation from tipping-bucket rain gauges was used to identify extreme precipitation events (Section 4), with an absolute measurement bias of ±0.2 mm under light rainfall conditions ($\leq$ 4 mm/h) and a relative bias within ±4% during heavy rainfall ($\geq$ 10 mm/h).

2.4 Atmospheric Priori

The ERA5 reanalysis dataset (Hersbach et al., 2020) is used in this study to provide the a priori atmospheric state for the retrieval of water vapor mass mixing ratio profiles. ERA5 offers dynamically consistent and physically constrained atmospheric fields by assimilating a comprehensive set of satellite and in situ observations within a state-of-the-art numerical weather prediction system. Given its extensive validation and widespread application, ERA5 is well suited for providing background information in variational retrieval frameworks. In this study, profiles of temperature, specific humidity, pressure, and geopotential height are extracted from ERA5 and interpolated to the observational sites using nearest-neighbour spatial interpolation. A temporal refinement is subsequently applied using an inverse distance weighting approach to better match the timing of the ground-based observations.

3 Adaptive Observation Weighting TCKF1D-Var

In our previous studies, we demonstrated that using virtual potential temperature as the control variable together with a ratio-based cost function allows more effective utilization of GMWR observations, producing temperature and humidity retrieval profiles that are more accurate than those obtained with the classical 1D-Var approach (Zhang et al., 2026a). Building on this work, we further applied the same approach to the MRL water vapor and nitrogen Raman channels, confirming the method’s applicability to MRL observations as well (Zhang et al., 2026b). The ratio-based cost function with virtual potential temperature as the control variable can be expressed as:

$$J_{(x)} = (\frac{H_{(x)}}{y} - 1)^2 + (\frac{\theta_{v(x)}}{\theta_{v(x_o)}} - 1)^2, \quad (1)$$

where x denotes the retrieval profile, $H_{(x)}$ is the observation operator (which differs depending on the type of observation, e.g., GMWR or MRL), θ_v is the virtual potential temperature calculated from the retrieved profiles, and x_o represents the atmospheric prior from ERA5 reanalysis. When the cost function is expanded to account for all observation channels (for GMWR) or vertical bins (for MRL), as well as the vertical resolution of the retrieval profiles, it becomes:

$$J_{(x)} = \sum_{i=1}^{m} (\frac{H^i_{(x)}}{y^i} - 1)^2 + \sum_{j=1}^{n} (\frac{\theta^j_{v\,(x)}}{\theta^j_{v\,(x)}} - 1)^2, \quad (2)$$

where m denotes the number of observation channels or vertical bins, and n is the number of vertical layers in the retrieval. This formulation underlies the static observation weighting TCKF-1D-Var described in sections 4.1 and 4.2. By introducing adjustable weights c^i for each observation i that can be diagnosed during the cost function minimization, the static formulation is generalized to the adaptive observation weighting TCKF-1D-Var:

$$J_{(x)} = \sum_{i=1}^{m} c^i (\frac{H^i_{(x)}}{y^i} - 1)^2 + \sum_{j=1}^{n} (\frac{\theta^j_{v\,(x)}}{\theta^j_{v\,(x)}} - 1)^2. \quad (3)$$

For the synergistic retrieval using both GMWR and MRL observations (section 4.3), the cost function is extended by including additional observation terms:

$$J_{(x)} = \sum_{k=1}^{m_{MRL}} (\frac{H^k_{MRL\,(x)}}{y^k_{MRL}} - 1)^2 + \sum_{i=1}^{m_{GMWR}} (\frac{H^i_{GMWR\,(x)}}{y^i_{GMWR}} - 1)^2 + \sum_{j=1}^{n} (\frac{\theta^j_{v\,(x)}}{\theta^j_{v\,(x)}} - 1)^2. \quad (4)$$

Introducing adaptive weights for each observation leads to the adaptive observation weighting formulation for the synergistic retrieval:

$$J_{(x)} = \sum_{k=1}^{m_{MRL}} c^k_{MRL} (\frac{H^k_{MRL\,(x)}}{y^k_{MRL}} - 1)^2 + \sum_{i=1}^{m_{GMWR}} c^i_{GMWR} (\frac{H^i_{GMWR\,(x)}}{y^i_{GMWR}} - 1)^2 + \sum_{j=1}^{n} (\frac{\theta^j_{v\,(x)}}{\theta^j_{v\,(x)}} - 1)^2. \quad (5)$$

As in our previous work (Zhang et al., 2026a and 2026b), the minimization of the cost function in this study is performed using the L-BFGS-B algorithm (Gerber and Furrer, 2019). This framework allows both single-instrument and synergistic retrievals to adaptively weight observations, improving the accuracy and consistency of the retrieved temperature and humidity profiles.

4 Results and discussion

Following our previous study (Zhang et al., 2026a and 2026b), nocturnal heavy precipitation events were defined as cases with an hourly accumulated precipitation amount ≥ 10 mm. To ensure a consistent comparison among the three sensitivity experiments based on GMWR-based retrievals (GMWROnly, Section 4.1), MRL-based retrievals (MRLOnly, Section 4.2), and GMWR–MRL synergistic retrievals (GMWRnMRL, Section 4.3), an additional data-availability constraint was imposed. Specifically, only events for which both the GMWR and MRL provided valid observations during the precipitation period were retained for analysis. As a consequence, the final sample size used in this study was reduced relative to that employed in Zhang et al. (2026a), resulting in a total of 107 nocturnal heavy precipitation cases. The statistical characteristics of the selected events are summarized in Table 1. Among the 56 observational sites included in the study, 26 sites experienced at least one nighttime heavy precipitation event that satisfied the selection criteria. To further characterize the intensity distribution of the selected cases, the events were categorized into three precipitation classes according to hourly accumulated precipitation (PI): 10 − 20 mm, 20–30 mm, and ≥30 mm. The majority of cases (82 events, approximately 76.6% of the total sample) fell within the 10–20 mm category, while 14 events (13.1%) were associated with hourly precipitation amounts between 20 and 30 mm. The remaining 11 events (10.3%) exceeded 30 mm.

Table 1. Nocturnal Heavy Precipitation Case Summary

Station			PI (mm)		Case Amount			
WMO ID	Latitude (degree)	Longitude (degree)	Maximum	Minimum	Total	PI ∈ [10 mm, 20mm)	PI ∈ [20 mm, 30mm)	PI ∈ [30 mm, +∞)
50953	45.93	126.57	31.4	22.7	3	0	1	2
53463	40.85	111.57	12.0	12.0	1	1	0	0
53845	36.58	109.45	15.9	15.9	1	1	0	0
54161	43.90	125.22	15.2	15.2	1	1	0	0
54340	41.66	123.32	23.8	10.3	2	1	1	0
56080	35.00	102.90	18.0	10.0	2	2	0	0
56187	30.75	103.86	18.1	18.1	1	1	0	0
56492	28.80	104.60	12.4	10.1	2	2	0	0
56571	27.90	102.27	20.9	20.9	1	0	1	0
56691	26.87	104.28	17.8	12.3	3	3	0	0
56739	24.98	98.51	15.2	10.1	2	2	0	0
56778	25.00	102.65	32.3	32.3	1	0	0	1
56964	22.79	100.96	25.8	10.7	6	4	2	0
57083	34.72	113.65	23.8	23.8	1	0	1	0
57461	30.74	111.36	51.4	18.7	6	2	1	3
57516	29.58	106.46	33.5	10.2	5	4	0	1
58150	33.75	120.30	38.7	10.0	7	4	2	1
58362	31.40	121.45	38.9	26.4	2	0	1	1

https://doi.org/10.5194/egusphere-2026-3341
Preprint. Discussion started: 9 July 2026

58424	30.62	116.97	28.1	10.2	6	5	1	0
58633	29.00	118.90	24.6	10.8	9	7	2	0
58725	27.33	117.47	36.7	12.2	2	1	0	1
58847	26.08	119.28	35.9	11.2	5	4	1	0
59211	23.90	106.60	14.1	11.0	5	5	0	0
59280	23.71	113.09	16.2	11.0	11	11	0	0
59293	23.79	114.73	19.2	10.0	10	10	0	0
59316	23.39	116.68	33.3	10.2	12	11	0	1

To quantitatively evaluate the retrieval performance of the adaptive observation weighting TCKF1D-Var and static observation weighting TCKF1D-Var frameworks, radiosonde observations are used as the reference dataset. The accuracy of the retrieved thermodynamic profiles is assessed using two commonly adopted statistical metrics: the mean bias (MB) and the root-mean-square error ($RMSE$). The MB is used to quantify the systematic deviation of the retrievals from the radiosonde observations, while the $RMSE$ provides a measure of the overall retrieval error by accounting for both systematic and random discrepancies. These metrics are calculated at each retrieval level by comparing the retrieved thermodynamic variables with the corresponding radiosonde observations according to:

$$MB = \overline{Ret - Raob}, \tag{6}$$

$$RMSE = \sqrt{\frac{\sum_{i=1}^{n}(Ret-Raob)^2}{n}}, \tag{7}$$

where Ret denotes the thermodynamic retrievals produced by either the adaptive observation weighting TCKF1D-Var or the static observation weighting TCKF1D-Var framework, $Raob$ represents the corresponding radiosonde observations, and n is the total number of matched retrieval–radiosonde profile pairs used in the statistical analysis, n denotes the sample amount.

4.1 Adaptive weighting for ground-based microwave radiometer retrievals

4.1.1 Retrieval performance of adaptive and static weighting schemes

As shown in Figure 2, GMWR observations can be effectively digested within both the adaptive observation weighting TCKF1D-Var and static observation weighting TCKF1D-Var frameworks to correct the prior temperature and water vapor mass mixing ratio profiles. However, the incorporation of the adaptive observation weighting strategy leads to a improved retrieval performance compared with the static weighting approach. For the temperature profiles, the MB distributions shown in Figure 2a demonstrate that both the GMWROnly Dynamic Weight retrievals (red line) generated by adaptive observation weighting TCKF1D-Var framewrok and the GMWROnly Static Weight retrievals (blue line) generated by static

https://doi.org/10.5194/egusphere-2026-3341
Preprint. Discussion started: 9 July 2026

observation weighting TCKF1D-Var framewrok produce smaller MB than the ERA5 prior profiles (black line). Nevertheless, the overall magnitude of the improvement remains relatively limited, with the reduction generally smaller than 0.02 K. Although the adaptive weighting strategy does not substantially alter the temperature MB structure, a more distinct advantage can be identified in the $RMSE$ results. As shown in Figure 2b, both retrieval schemes reduce the temperature RMSE relative to the ERA5 prior, while the GMWROnly Dynamic Weight retrievals consistently outperform the GMWROnly Static Weight retrievals. This improvement is particularly evident between 900 and 4800 meters above ground level, where the $RMSE$ reduction reaches approximately 0.02 K. These results suggest that the adaptive observation weighting strategy can provide a more balanced utilization of GMWR observations and background constraints, thereby improving the stability and accuracy of the temperature retrievals. Compared with temperature, the influence of GMWR observations on the water vapor mass mixing ratio retrievals is more pronounced. As illustrated in Figure 2c, both the GMWROnly Dynamic Weight and GMWROnly Static Weight retrievals exhibit substantially smaller MB than the ERA5 prior profiles. More importantly, the adaptive observation weighting approach further reduces the MB relative to the static weighting method, with the most significant improvements occurring between 600 and 4800 meters. The maximum reduction in MB reaches approximately 0.08 g/kg near 2700 meters. The $RMSE$ distributions of the water vapor mass mixing ratio profiles shown in Figure 2d further support this conclusion. Consistent with the MB analysis, the GMWROnly Dynamic Weight retrievals exhibit systematically smaller $RMSE$ values than the GMWROnly Static Weight retrievals throughout most of the troposphere. Although the maximum magnitude of the $RMSE$ improvement (approximately 0.05 g/kg at 2700 meters above ground) is smaller than that of the MB reduction, indicating that the adaptive observation weighting strategy improves the overall bias characteristics of the moisture retrievals. The results demonstrate that both TCKF1D-Var retrieval schemes can utilize GMWR observations to refine the prior thermodynamic profiles generated from ERA5 reanalysis, while the adaptive observation weighting strategy introduces an additional level of flexibility that enhances the retrieval performance.

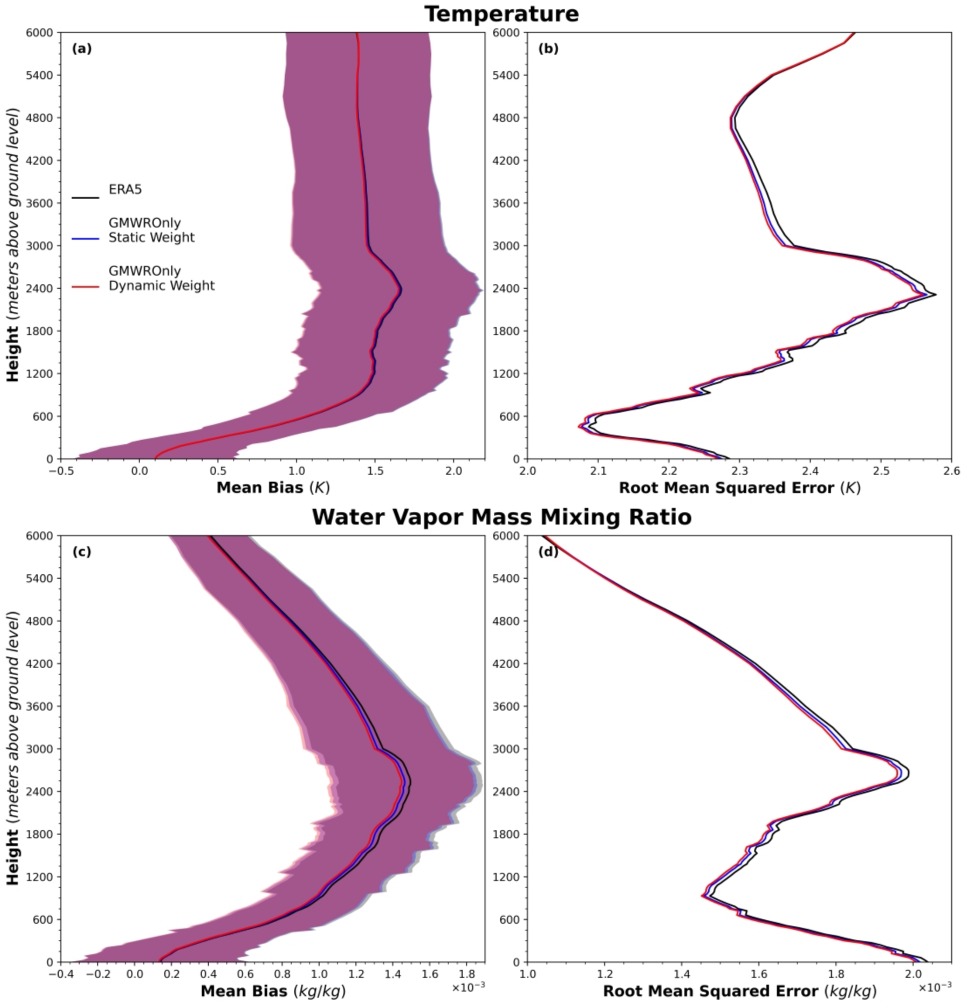

Figure 2. Vertical distributions of the retrieval errors for temperature and water vapor mass mixing ratio profiles obtained using the ERA5 prior profiles, the GMWROnly Static Weight retrievals, and the GMWROnly Dynamic Weight retrievals. Panels (a) and (b) show the MB and $RMSE$ of the temperature profiles, respectively, while panels (c) and (d) present the corresponding MB and $RMSE$ for the water vapor mass mixing ratio profiles. The black lines denote the ERA5 prior profiles, the blue lines represent the GMWROnly Static Weight retrievals based on the static observation weighting TCKF1D-Var method, and the red lines indicate the GMWROnly Dynamic Weight retrievals derived from the adaptive observation weighting TCKF1D-Var method. The shaded areas indicate the 95% confidence intervals for the ERA5 (gray), GMWROnly Static Weight (blue), and GMWROnly Dynamic Weight (red) retrievals.

To further investigate the performance of the adaptive observation weighting strategy under different precipitation intensities, the validation cases were stratified according to hourly accumulated precipitation. The resulting error statistics are presented in Figure 3. For cases associated with PI between 10 and 20 mm, the vertical distributions and magnitudes of both the MB (Figure 3a, c) and $RMSE$ (Figure 3b, d) closely resemble those obtained from the overall evaluation shown in Figure 2. This consistency is expected because this precipitation category accounts for 76.6% of all validation samples and therefore dominates the aggregate statistics. As a result, the performance characteristics identified in the overall assessment are largely representative of this subset. For cases with PI between 20 and 30 mm, the benefit of the adaptive observation weighting strategy becomes more variable. In terms of temperature retrieval, the differences between the adaptive and static weighting approaches are negligible in the MB profiles (Figure 3e), while a discernible reduction in $RMSE$ is observed only between approximately 3.0 and 4.8 km above ground level (Figure 3f). In contrast, more substantial improvements are evident in the water vapor mass mixing ratio retrievals. The adaptive observation weighting TCKF1D-Var framework consistently produces smaller water vapor mass mixing ratio MBs below 4.8 km (Figure 3g), indicating a more effective correction of the prior-state biases. A similar behavior is found in the $RMSE$ profiles (Figure 3h), although the altitude range exhibiting noticeable improvement is reduced to approximately 4.2 km above ground level. For heavy-rainfall cases with PI exceeding 30 mm, the superiority of the adaptive observation weighting strategy becomes considerably less apparent. The temperature retrieval results show little difference between the adaptive and static weighting schemes in either MB (Figure 3i) or $RMSE$ (Figure 3j). Similar conclusions can be drawn for water vapor mass mixing ratio retrievals. Although both weighting schemes are capable of reducing the MB and $RMSE$ relative to the prior profiles by using GMWR observations (Figure 3k, l), the available evidence does not indicate a statistically meaningful advantage of the adaptive observation weighting approach over the conventional static weighting method. Therefore, under the most intense precipitation conditions examined in this study, the adaptive weighting strategy does not provide a clear additional benefit for improving the accuracy of retrieved thermodynamic profiles. The reduced advantage of the adaptive weighting strategy during the most intense precipitation events may be associated with the increased uncertainty of GMWR observations under heavy rainfall conditions, which limits the effectiveness of dynamically adjusting observational error statistics (Böck et al., 2025).

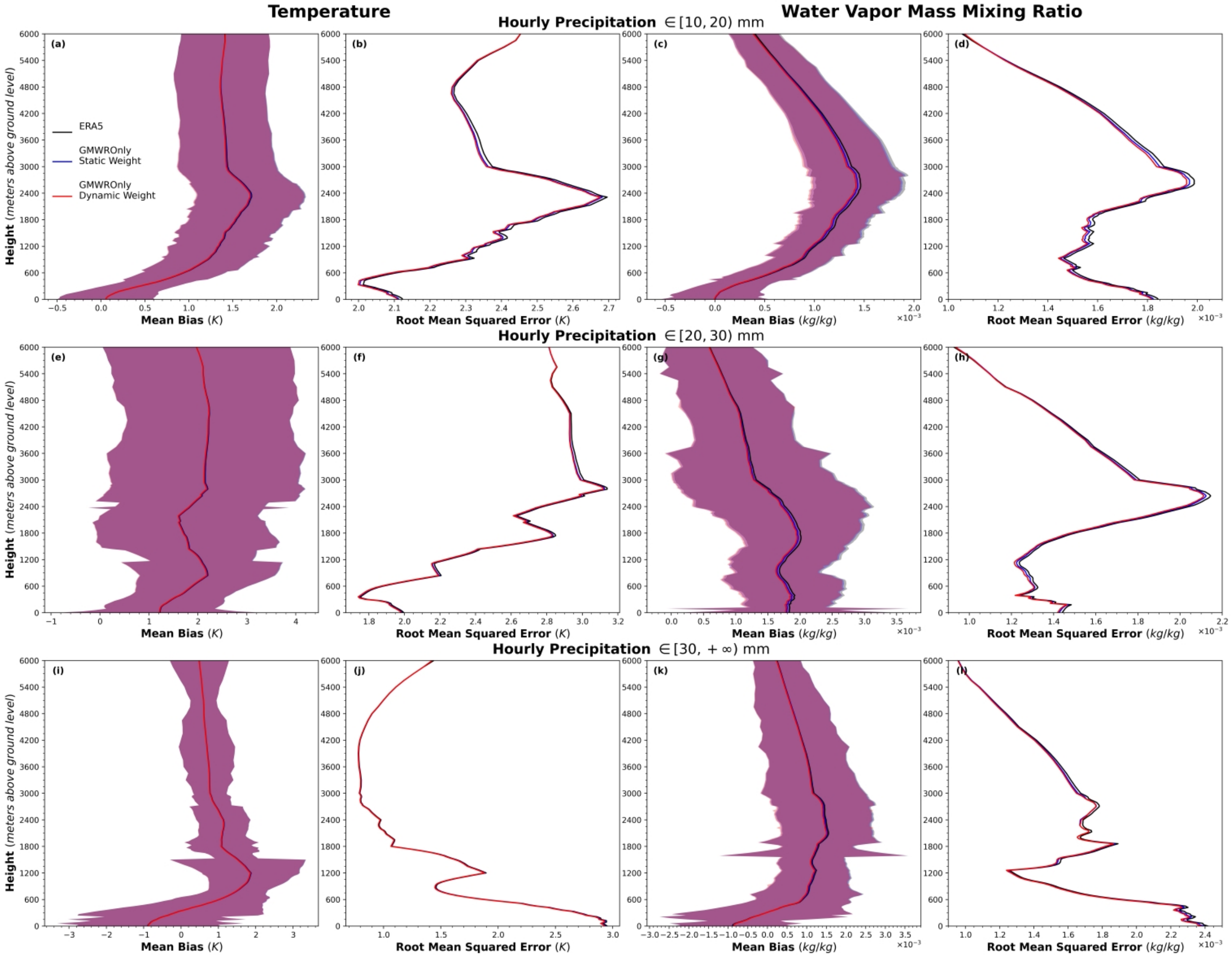

Figure 3. Vertical distributions of temperature and water vapor mass mixing ratio retrieval errors for the adaptive observation weighting and static observation weighting TCKF1D-Var frameworks under different precipitation intensities. Panels (a–d) show the MB and $RMSE$ profiles for cases with hourly accumulated precipitation of 10 – 20 mm. Panels (e – h) show the corresponding results for cases with hourly accumulated precipitation of 20–30 mm. Panels (i–l) present the results for cases with hourly accumulated precipitation exceeding 30 mm. Temperature retrieval statistics are shown in panels (a, b, e, f, i, j), while water vapor mass mixing ratio retrieval statistics are shown in panels (c, d, g, h, k, l). The gray, blue, and red curves represent the prior profiles, the static observation weighting TCKF1D-Var retrievals, and the adaptive observation weighting TCKF1D-Var retrievals, respectively. Shaded regions indicate the 95 % confidence intervals.

4.1.2 Adaptive channel weighting characteristics

The preceding experiments demonstrated that the adaptive observation weighting TCKF1D-Var framework generally produces more accurate thermodynamic profiles than both the static observation weighting TCKF1D-Var framework and the corresponding prior profiles for most nocturnal heavy precipitation cases. To better understand the origin of these improvements, it is necessary to examine how individual channels are weighted within the adaptive retrieval framework.

https://doi.org/10.5194/egusphere-2026-3341
Preprint. Discussion started: 9 July 2026

Figure 4 presents boxplots of the channel weights assigned by the adaptive observation weighting TCKF1D-Var method for the nine channels used in this study. Considering all heavy precipitation cases together (Figure 4a), clear differences can be identified among the four water vapor channels (22.235, 23.035, 23.835, and 26.235 GHz). The first three channels are consistently assigned relatively large weights, with both median values and mean values exceeding 90 %. Furthermore, the small differences between the medians and means indicate that their contributions remain relatively stable across different atmospheric conditions. Although several outliers are present, they account for less than 10 % of the total samples and therefore have only a limited influence on the overall statistics. In contrast, the 26.235 GHz channel exhibits both lower median and mean weights, suggesting a reduced contribution to the retrieval accuracy. The larger discrepancy between its median and mean values further indicates a stronger sensitivity of its information content to environmental conditions. A similar pattern is found among the oxygen absorption channels. The three higher-frequency channels (53.85, 54.94, and 56.66 GHz) receive consistently large weights, with median and mean values generally exceeding 90 %, implying substantial and robust contributions to thermodynamic profile retrievals. Conversely, the lower-frequency channels (51.25 and 52.28 GHz) are assigned noticeably smaller weights. The larger separation between their median and mean values also suggests that their contributions vary more strongly among different precipitation events.

For cases with PI between 10 and 20 mm (Figure 4b), the statistical characteristics are nearly identical to those obtained from the complete dataset (Figure 4a). The channels centered at 22.235, 23.035, 23.835, 53.85, 54.94, and 56.66 GHz consistently receive larger weights than the 26.235, 51.25, and 52.28 GHz channels, indicating that these six channels provide the dominant observational constraints on the thermodynamic retrievals. Moreover, the close agreement between median and mean weights suggests that their contributions remain relatively stable under varying atmospheric conditions. The results for the 20–30 mm precipitation category (Figure 4c) retain the overall characteristics observed in Figure 4a, although noticeable differences appear in the weight distributions of the 26.235, 51.25, and 52.28 GHz channels. For these channels, the mean weights are located close to the first quartile, whereas the median values are much closer to the third quartile. This behavior is primarily attributable to the combined effects of a limited sample size (14 cases) and a relatively large number of outliers, both of which increase the sensitivity of the statistics to individual events. Despite a similarly limited sample size for the most intense precipitation category (≥30 mm; 11 cases), the channel-weight distributions shown in Figure 4d remain more consistent with the overall statistics than those in Figure 4c, indicating that the dominant channel-ranking characteristics are largely preserved even under the strongest precipitation conditions examined in this study.

An additional feature worth noting is that none of the channels exhibit weights approaching 100 % for all cases. This indicates that the information content contained in the GMWR observations is not fully utilized by the adaptive observation weighting framework. Nevertheless, because the adaptive observation weighting TCKF1D-Var retrievals generally outperform the corresponding static-weighting retrievals, the discarded portion of the observations can reasonably be interpreted as residual observational information with limited relevance to atmospheric temperature and humidity retrievals.

Whether these residuals still contain useful thermodynamic information, especially for the 26.235, 51.25, and 52.28 GHz channels, and to what extent such information could be exploited by future retrieval algorithms, remains an open question that warrants further investigation.

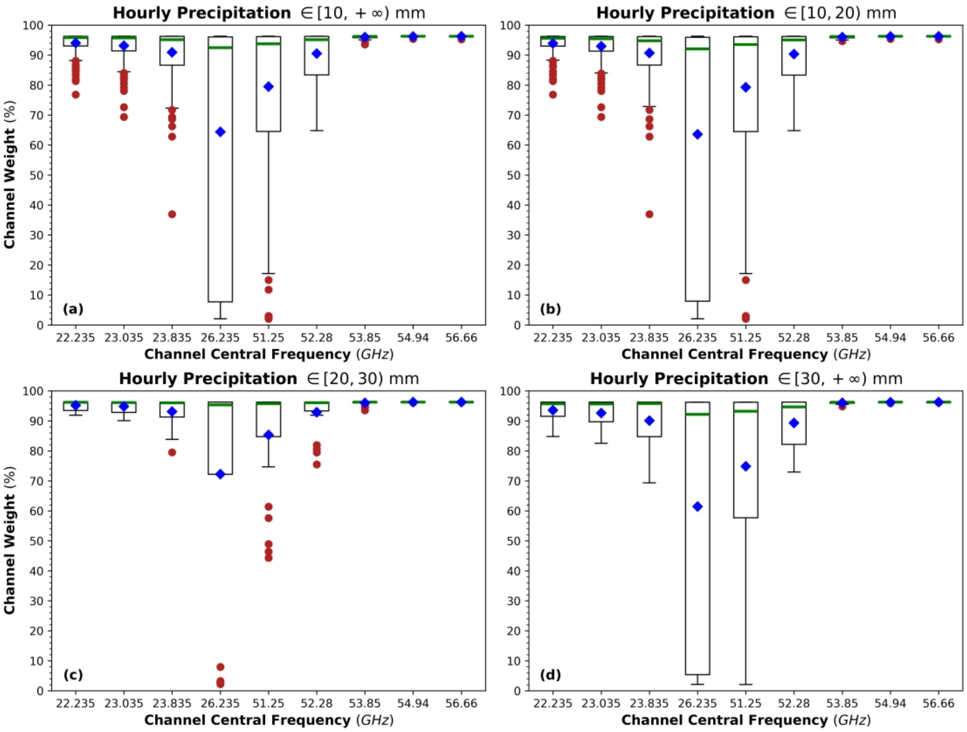

Figure 4. Boxplots of the adaptive observation weights assigned to the 9 GMWR channels by the adaptive observation weighting TCKF1D-Var framework. Results are shown for (a) all nocturnal heavy precipitation cases, (b) cases with hourly accumulated precipitation between 10 and 20 mm, (c) cases with hourly accumulated precipitation between 20 and 30 mm, and (d) cases with hourly accumulated precipitation exceeding 30 mm. The boxes represent the interquartile range (IQR), with the lower and upper edges corresponding to the first and third quartiles, respectively. The green horizontal lines indicate the median values, while the blue squares denote the mean values. Whiskers extend to 1.5 times the IQR, and red dots represent outliers beyond this range.

4.2 Adaptive weighting for Mie–Raman lidar retrievals

4.2.1 Retrieval performance evaluation

The adaptive observation weighting TCKF1D-Var framework also demonstrates an enhanced capability to correct prior thermodynamic profiles when using MRL observations (Figure 5). Similar to the results obtained from the GMWR experiments (Figure 2a, b), both the adaptive and static observation weighting schemes improve the temperature retrievals relative to the prior profiles. However, the magnitude of the improvement remains limited. The reductions in both temperature MB (Figure 5a) and $RMSE$ (Figure 5b) are relatively small, indicating that the MRL observations provide only modest additional constraints on the temperature profile. Furthermore, the advantage of the adaptive observation weighting framework over the static weighting framework is only marginally discernible and is primarily reflected in the $RMSE$ profiles (Figure 5b), where slightly smaller retrieval errors are obtained throughout part of the atmospheric column. In contrast, the benefits of the adaptive weighting strategy are more evident for water vapor mass mixing ratio retrievals. Compared with the prior profiles, the adaptive observation weighting TCKF1D-Var framework reduces both the MB and $RMSE$ of the retrieved water vapor mass mixing ratio by up to approximately 0.1 g/kg (Figure 5c, d). Although the static observation weighting TCKF1D-Var framework also improves the prior water vapor mass mixing ratio profiles, its error reductions are generally smaller than those achieved by the adaptive weighting approach. Consequently, the adaptive observation weighting strategy appears to make more effective use of the humidity information contained in the MRL observations, resulting in a consistently improved representation of the atmospheric moisture structure. The stronger impact on humidity retrievals than on temperature retrievals is physically consistent with the fact that the MRL observations provide direct information on atmospheric water vapor, whereas temperature information is introduced only indirectly through the retrieval framework.

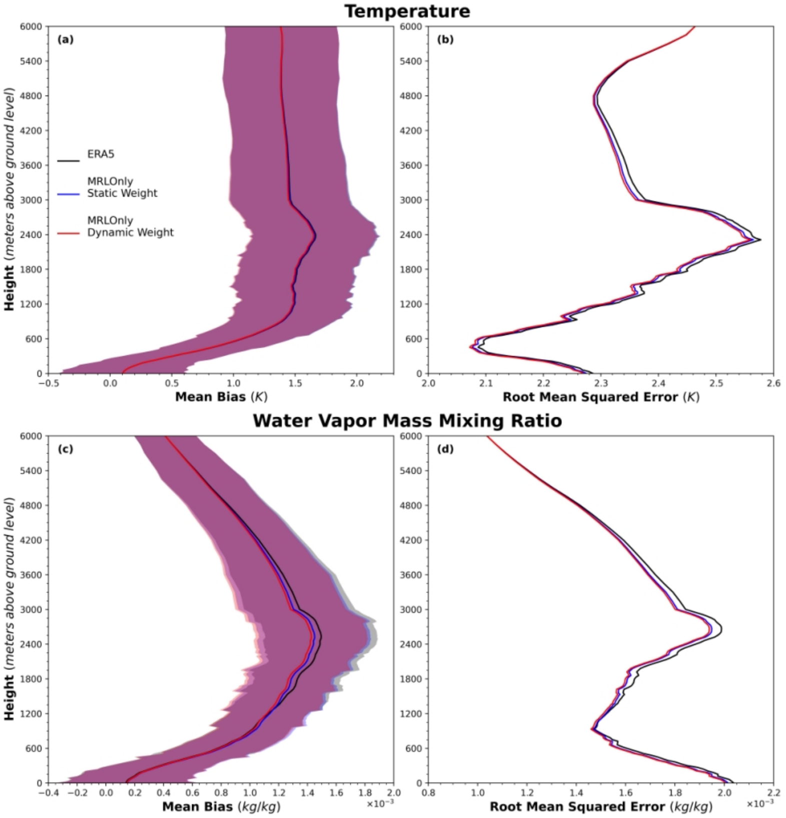

Figure 5. Same as Figure 2, but for retrievals based on MRL observations. Panels (a) and (b) show the vertical distributions of temperature MB and $RMSE$, respectively, while panels (c) and (d) show the corresponding statistics for water vapor mixing

https://doi.org/10.5194/egusphere-2026-3341
Preprint. Discussion started: 9 July 2026

ratio. Gray, blue, and red curves represent the prior profiles, static observation weighting TCKF1D-Var retrievals, and adaptive observation weighting TCKF1D-Var retrievals, respectively. Shaded regions indicate the 95 % confidence intervals.

The performance of the adaptive observation weighting TCKF1D-Var framework based on MRL observations for different precipitation categories is summarized in Figure 6. Overall, the stratified evaluation results are broadly consistent with the general performance assessment presented in Figure 5, indicating that the retrieval characteristics identified from the complete dataset remain valid across different precipitation intensities. For cases with PI between 10 and 20 mm, both the adaptive and static observation weighting frameworks exhibit error reductions that closely resemble those obtained from the overall evaluation. The magnitudes and vertical distributions of the temperature and water vapor mass mixing ratio MB (Figure 6a, c) and $RMSE$ (Figure 6b, d) are generally consistent with those shown in Figure 5, suggesting that this precipitation category largely governs the overall retrieval statistics. For cases with PI between 20 and 30 mm, the impact of MRL observations on temperature retrievals remains limited. As illustrated by the temperature MB profiles (Figure 6e), neither the adaptive nor the static observation weighting framework produces substantial corrections to the prior temperature profiles. A similar conclusion can be drawn from the temperature $RMSE$ profiles (Figure 6f). Although a slight reduction in $RMSE$ is evident, the magnitude of the improvement is considerably smaller than that obtained from the corresponding GMWR-based retrievals (Figure 3f) and remains practically negligible. In contrast, more pronounced improvements are observed in the retrievals of water vapor mass mixing ratio. Both frameworks reduce the errors relative to the prior profiles, while the adaptive observation weighting TCKF1D-Var framework consistently achieves smaller MBs and $RMSE$s than the static observation weighting approach (Figure 6g, h), indicating a more effective utilization of the humidity information provided by the MRL observations. The results for cases with PI exceeding 30 mm further reinforce this behavior. For temperature retrievals, the corrections to both the MB (Figure 6i) and $RMSE$ (Figure 6j) remain marginal, and the differences between the adaptive and static weighting schemes are small. This finding is consistent with the corresponding GMWR-based results shown in Figure 3i and j. In contrast, the adaptive observation weighting framework produces larger reductions in both the MB (Figure 6k) and $RMSE$ (Figure 6l) of the retrieved water vapor mass mixing ratio than the static observation weighting framework. Therefore, even under the most intense precipitation conditions considered in this study, the primary advantage of the adaptive observation weighting strategy remains its enhanced capability to improve the retrieval of atmospheric moisture profiles, whereas its influence on temperature retrievals is comparatively limited.

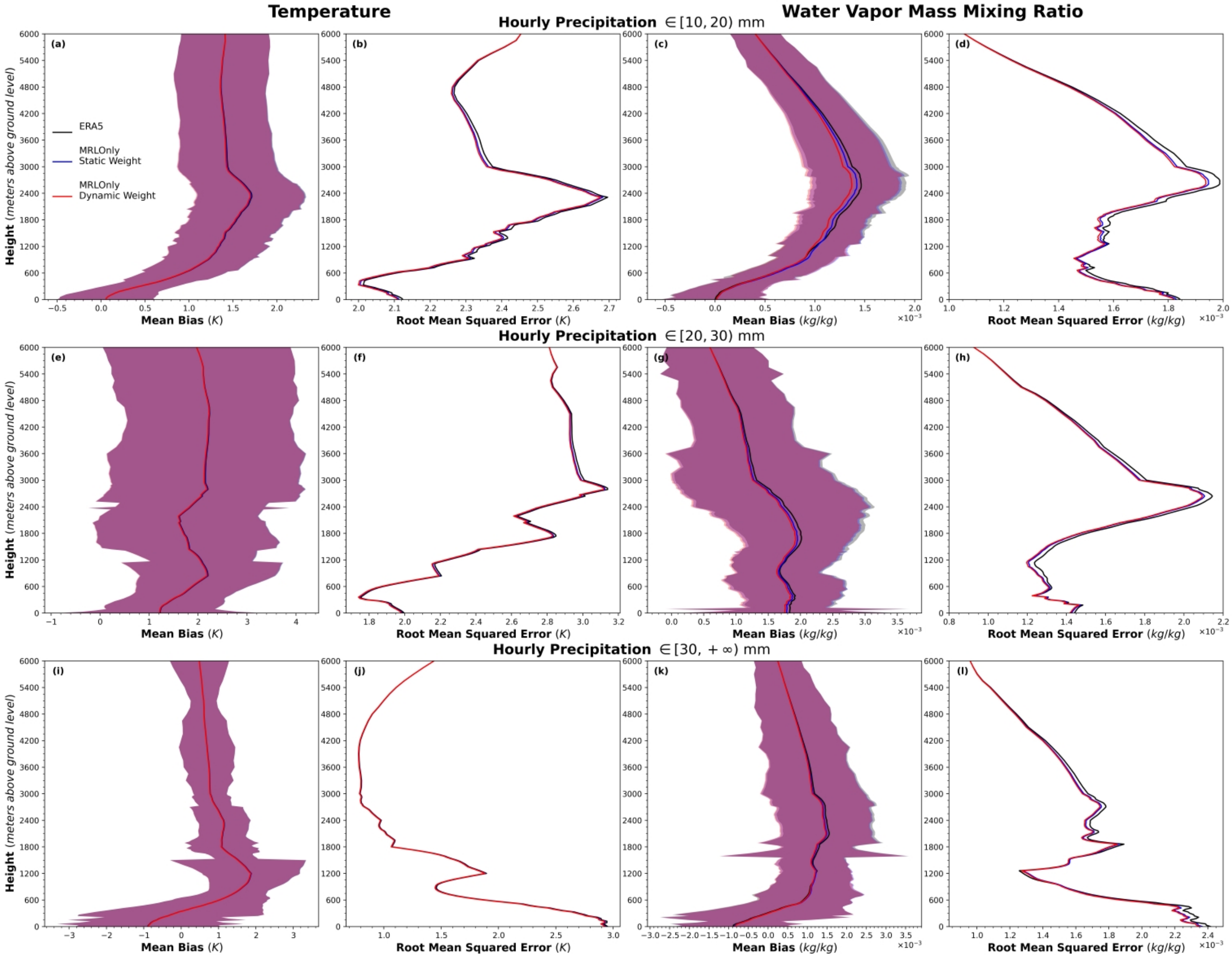

Figure 6. Same as Figure 3, but for retrievals based on MRL observations. Panels (a–d) show the MB and $RMSE$ profiles of temperature and water vapor mass mixing ratio retrievals for cases with hourly accumulated precipitation of 10–20 mm. Panels (e–h) show the corresponding results for cases with hourly accumulated precipitation of 20–30 mm, while panels (i–l) present the results for cases with hourly accumulated precipitation exceeding 30 mm. Temperature retrieval statistics are shown in panels (a, b, e, f, i, j), and water vapor mass mixing ratio retrieval statistics are shown in panels (c, d, g, h, k, l). Gray, blue, and red curves denote the prior profiles, static observation weighting TCKF1D-Var retrievals, and adaptive observation weighting TCKF1D-Var retrievals, respectively. Shaded regions indicate the 95 % confidence intervals.

4.2.2 Vertical variability of adaptive weights

Following the analysis strategy adopted in Section 4.1.2 for the GMWR observations, the vertical distributions of the adaptive observation weights assigned to MRL observations were examined using boxplots (Figure 7). For the complete set of heavy precipitation cases (Figure 7a), both the median weights and the mean weights exhibit a clear increase with height. This feature is particularly evident in the mean values, which reveal a transition around 1200 meters above ground level. Below this altitude, the weights diagnosed by the adaptive observation weighting framework remain relatively stable, generally ranging between 96 % and 97 %. Above 1200 meters, the average weights exceed 97 % and remain consistently high throughout the remainder of the profile. In addition to the increase in weight magnitude, the variability of the diagnosed weights also changes with height. The differences between the median and mean values are noticeably larger below 1200 meters than above, suggesting a stronger dependence of the assigned weights on atmospheric conditions in the lower troposphere. This interpretation is further supported by the larger number of outliers observed below 1200 meters, indicating more pronounced variability in the utilization of MRL observations near the surface.

The results for cases with hourly accumulated precipitation between 10 and 20 mm (Figure 7b) closely resemble those obtained from the full dataset. Both the overall magnitude of the weights and their vertical structure are nearly identical to those shown in Figure 7a. As discussed for the GMWR experiments, this similarity is expected because the 10–20 mm precipitation category accounts for 76.6 % of all validation cases and therefore dominates the aggregate statistics. For cases with hourly accumulated precipitation between 20 and 30 mm (Figure 7c), the general tendency of increasing weights with height is still evident. However, the transition altitude shifts downward to approximately 450 m above ground level. In addition, localized decreases in the mean weights are observed near 1.2 km and 2.4 km, producing noticeable discontinuities in the otherwise smooth vertical structure. These features suggest that the contribution of MRL observations to the retrieval process becomes more height-dependent under stronger precipitation conditions. A similar downward shift of the transition altitude is also found for the most intense precipitation events (Figure 7d). Although the overall "lower-weight–higher-weight" pattern remains evident, the transition occurs at approximately 600 m above ground level, substantially lower than that identified from the complete dataset. Despite the relatively limited sample size of this precipitation category, the persistence of this feature indicates that the vertical distribution of the diagnosed observation weights may vary systematically with precipitation intensity. Such behavior suggests that the adaptive observation weighting framework adjusts the utilization of MRL observations in response to changing atmospheric conditions, particularly within the lower troposphere where precipitation-related processes are most active.

The phenomenon that observed increase in adaptive observation weights with height may be related to the altitude-dependent characteristics of the MRL observations. In the lower atmosphere, particularly within the planetary boundary layer, the thermodynamic environment is strongly influenced by local moisture transport, turbulent mixing, surface heterogeneity, and precipitation-related processes (Zhang et al., 2018; Ma et al., 2026). These factors can introduce substantial spatial and temporal variability into the observed humidity field, leading to larger observation residuals and increased uncertainty in the retrieval process. Consequently, the adaptive weighting framework tends to assign relatively lower and more variable weights to MRL observations in the lower troposphere. At higher altitudes, the atmospheric environment is generally less affected by near-surface processes and exhibits smoother vertical structures. Under such conditions, the consistency between the observations and the retrieval framework tends to improve, resulting in smaller observation residuals and more stable estimates of the observation information content. This behavior is reflected by the higher median and mean weights as well as the reduced number of outliers observed above the transition altitude in Figure 7. Therefore, the diagnosed vertical distribution of observation weights suggests that the adaptive observation weighting framework dynamically adjusts its confidence in MRL observations according to the altitude-dependent characteristics of the atmospheric moisture field. It should be noted, however, that the adaptive weights are determined jointly by the observation residuals, background-state uncertainties, and the retrieval framework itself. Therefore, the mechanisms discussed above should be regarded as plausible interpretations rather than definitive explanations. Additional investigations based on observation-error diagnostics and information-content analyses would be required to fully quantify the physical processes responsible for the observed vertical weight distributions.

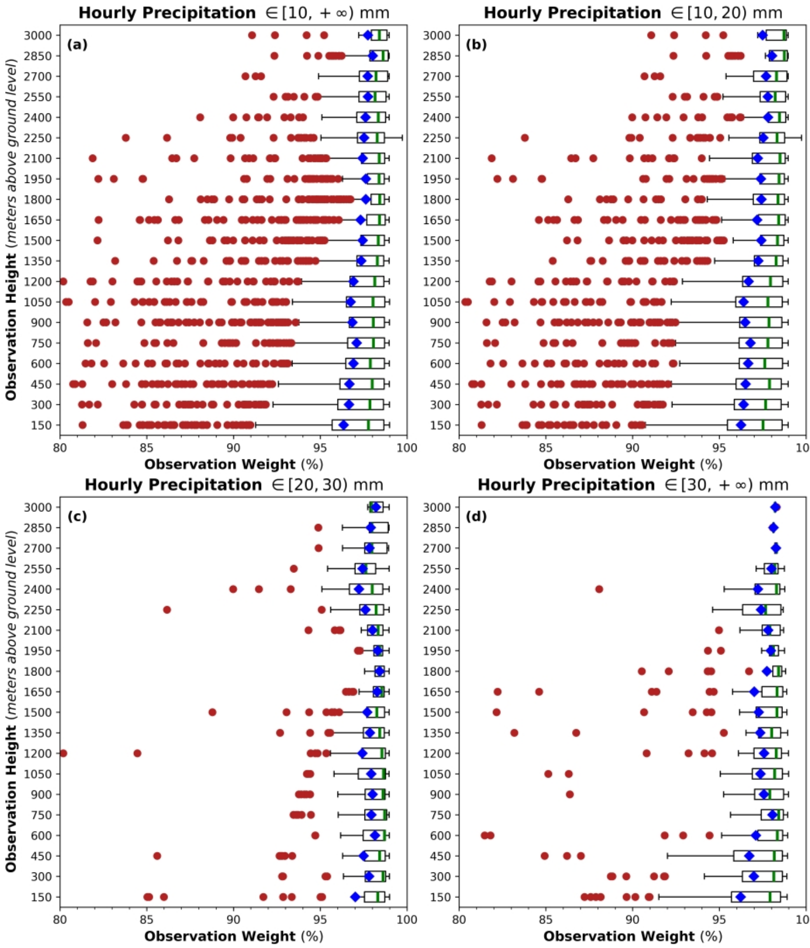

Figure 7. Statistical distributions of observation weights diagnosed by the adaptive observation weighting TCKF1D-Var framework for MRL observations at different heights. Panels (a)–(d) correspond to all nocturnal heavy precipitation cases, cases with hourly accumulated precipitation of 10–20 mm, 20–30 mm, and >30 mm, respectively. The box boundaries indicate the first and third quartiles, the green vertical lines denote the medians, and the blue squares indicate the means. Whiskers extend to 1.5 times the interquartile range, and red dots denote outliers.

https://doi.org/10.5194/egusphere-2026-3341
Preprint. Discussion started: 9 July 2026

4.3 Adaptive weighting in synergistic multi-sensor retrievals

4.3.1 Synergistic retrieval performance of multi-sensor observations

Sections 4.1 and 4.2 demonstrated that, when using either GMWR or MRL observations individually, the adaptive observation weighting TCKF1D-Var framework generally produces thermodynamic retrievals with lower MBs and $RMSE$s than those obtained using the static observation weighting framework. The improvements are particularly evident for the retrieval of water vapor mass mixing ratio. An important question is whether these advantages are maintained when the two observing systems are combined within a unified retrieval framework. To address this issue, the performance of the adaptive and static observation weighting schemes under GMWR–MRL synergistic retrieval condition is examined in this section. Figure 8 summarizes the retrieval errors obtained from the synergistic inversion of GMWR and MRL observations. Similar to the results obtained from the single-instrument experiments (Figures 2a and 5a), both retrieval frameworks improve the prior temperature profiles, while the differences in temperature MB between the adaptive and static weighting schemes remain relatively small (Figure 8a). In contrast, a more noticeable advantage of the adaptive observation weighting framework is apparent in the temperature $RMSE$ profiles (Figure 8b), where the adaptive scheme consistently achieves smaller retrieval errors than the static weighting approach throughout much of the atmospheric column. The benefits of adaptive observation weighting are more pronounced for the retrieval of water vapor mass mixing ratio. As shown in Figure 8c and d, both the MB and $RMSE$ obtained from the adaptive observation weighting TCKF1D-Var framework are smaller than those produced by the static observation weighting framework. This result is consistent with the findings from the individual GMWR and MRL experiments (Figures 2c, d and 5c, d), further demonstrating the ability of the adaptive weighting strategy to make more effective use of water vapor-related observational information. A comparison between the synergistic retrieval results and the corresponding single-instrument retrievals reveals an additional benefit of combining GMWR and MRL observations. Relative to the retrievals based on either GMWR or MRL observations alone, the joint retrievals exhibit further reductions in both the MB and $RMSE$ of water vapor mass mixing ratio, with the improvement reaching approximately 0.02 g/kg. Importantly, this enhancement is observed in both the adaptive and static weighting frameworks, indicating that the complementary information provided by the two observing systems contributes to a more accurate characterization of the atmospheric thermodynamic structure. The fact that the adaptive observation weighting framework consistently achieves the lowest retrieval errors among all experiments further suggests that dynamically adjusting observational weights remains beneficial even when multiple observation types are assimilated simultaneously.

https://doi.org/10.5194/egusphere-2026-3341
Preprint. Discussion started: 9 July 2026

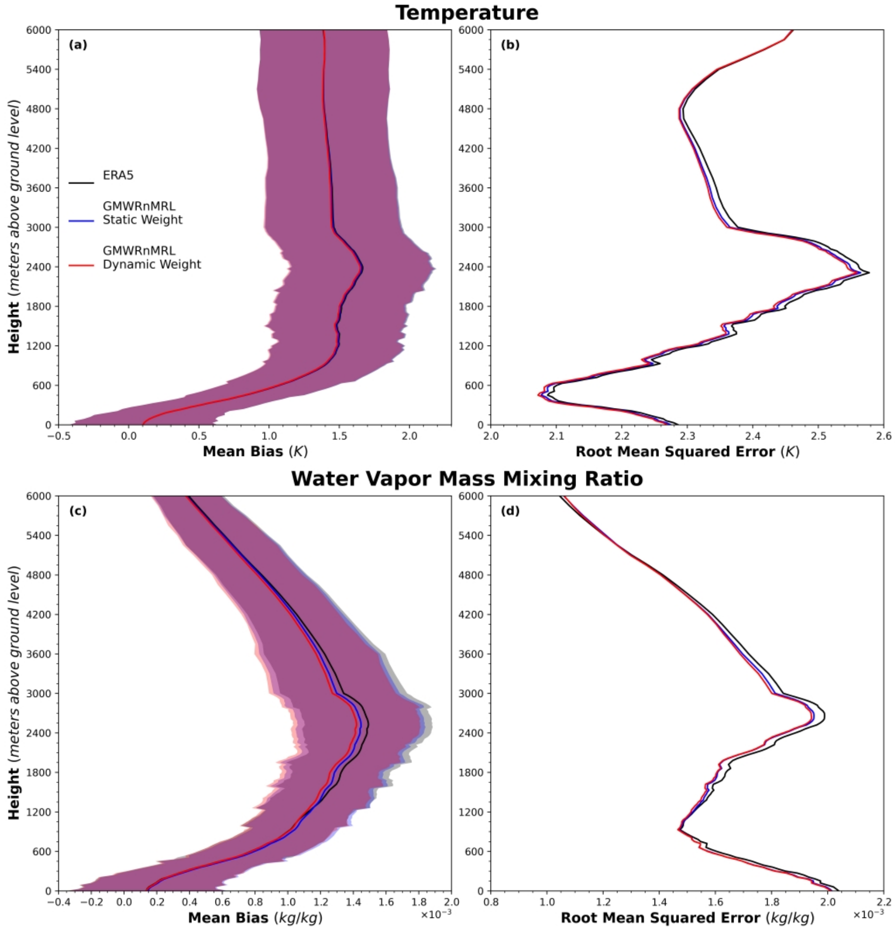

Figure 8. Same as Figures 2 and 5, but for retrievals based on the synergistic assimilation of GMWR and MRL observations. Panels (a) and (b) show the vertical distributions of temperature MB and $RMSE$, respectively, while panels (c) and (d) show the corresponding statistics for water vapor mass mixing ratio. Gray, blue, and red curves represent the prior profiles, static observation weighting TCKF1D-Var retrievals, and adaptive observation weighting TCKF1D-Var retrievals, respectively. Shaded regions indicate the 95 % confidence intervals.

The retrieval performance stratified by precipitation intensity for the GMWR–MRL synergistic experiments is presented in Figure 9. Overall, the results are broadly consistent with those obtained from the single-instrument experiments (Figures 3 and 6), indicating that the principal retrieval characteristics identified for the adaptive observation weighting framework remain robust when multiple observation types are assimilated simultaneously. For cases with PI between 10 and 20 mm, the vertical distributions of both the MB (Figure 9a, c) and root-mean-square error $RMSE$ (Figure 9b, d) closely resemble those obtained from the overall evaluation shown in Figure 8. This similarity is expected because this precipitation category represents the majority of the validation dataset and therefore dominates the aggregate statistics. Consequently, the retrieval characteristics observed in the overall assessment are largely representative of the 10–20 mm precipitation subset. For cases with PI between 20 and 30 mm, the improvements in temperature retrievals remain relatively modest. Both the adaptive and static observation weighting frameworks produce only limited reductions in temperature errors, with the reductions in $RMSE$ (Figure 9f) being slightly larger than those in MB (Figure 9e). Within this precipitation category, the superiority of the adaptive observation weighting framework over the static weighting framework is only marginally evident and is primarily reflected in the temperature $RMSE$ profiles. In contrast, the advantages of adaptive weighting are more apparent for the retrieval of water vapor mass mixing ratio. The adaptive observation weighting TCKF1D-Var framework consistently yields smaller MBs (Figure 9g) and $RMSE$s (Figure 9h) than the corresponding static observation weighting framework, indicating a more effective utilization of the complementary humidity information provided by the GMWR and MRL observations. For the most intense precipitation cases, with PI exceeding 30 mm, the relative performance differences between the two retrieval frameworks become most apparent in the retrieval of atmospheric moisture. Although both frameworks improve the prior thermodynamic profiles, the adaptive observation weighting approach produces noticeably smaller errors in the retrieved water vapor mass mixing ratio. This advantage is particularly evident in the $RMSE$ profiles (Figure 9l), where the separation between the adaptive and static weighting retrievals is most clearly expressed. These results further support the conclusion that the primary benefit of the adaptive observation weighting strategy lies in its enhanced ability to extract water vapor-related information from the assimilated observations, while the corresponding improvements in temperature retrievals remain comparatively limited.

https://doi.org/10.5194/egusphere-2026-3341
Preprint. Discussion started: 9 July 2026

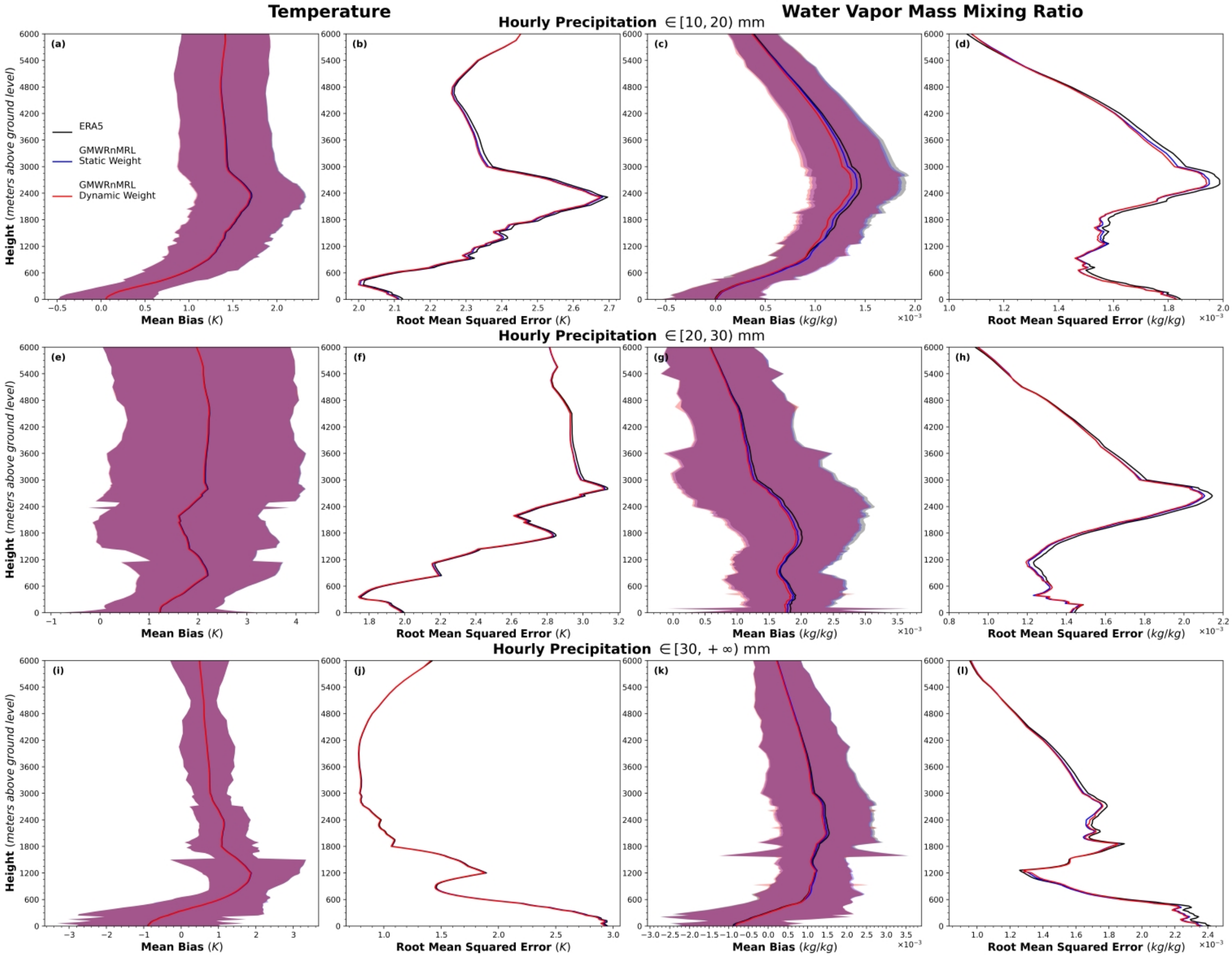

Figure 9. Same as Figures 3 and 6, but for retrievals based on the synergistic assimilation of GMWR and MRL observations. Panels (a−d) show the MB and $RMSE$ profiles of temperature and water vapor mass mixing ratio retrievals for cases with hourly accumulated precipitation of 10−20 mm. Panels (e−h) show the corresponding results for cases with hourly accumulated precipitation of 20–30 mm, while panels (i–l) present the results for cases with hourly accumulated precipitation exceeding 30 mm. Temperature retrieval statistics are shown in panels (a, b, e, f, i, j), and water vapor mass mixing ratio retrieval statistics are shown in panels (c, d, g, h, k, l). Gray, blue, and red curves denote the prior profiles, static observation weighting TCKF1D-Var retrievals, and adaptive observation weighting TCKF1D-Var retrievals, respectively. Shaded regions indicate the 95 % confidence intervals.

To quantitatively assess the contributions of the adaptive observation weighting and static observation weighting TCKF1D-Var frameworks to thermodynamic profile retrievals, bias reduction rates were calculated for both the MB and $RMSE$. For MB, the reduction rate is defined as $\sum (MB_{Analysis} - MB_{ERA5}) \big/ \sum MB_{ERA5}$, where $MB_{Analysis}$ denotes the mean bias of the retrievals produced by either the adaptive or static observation weighting framework, and MB_{ERA5} represents the corresponding mean bias of the ERA5 prior profiles. Similarly, the $RMSE$ reduction rate is defined as

$\sum(RMSE_{Analysis} - RMSE_{ERA5}) / \sum RMSE_{ERA5}$, where $RMSE_{Analysis}$ and $RMSE_{ERA5}$ denote the $RMSE$s of the retrieval and prior profiles, respectively. According to these definitions, negative values indicate that the retrieval framework reduces the corresponding error relative to the prior profile, while larger absolute values correspond to more detectable improvements.

Table 2 summarizes the temperature MB and $RMSE$ reduction rates for the GMWROnly, MRLOnly, and GWMRnMRL retrievals across different precipitation categories as well as for the complete heavy-precipitation dataset. Overall, the adaptive observation weighting TCKF1D-Var framework consistently achieves larger reductions in both MB and $RMSE$ than the static observation weighting framework, confirming its superior ability to improve temperature profile retrievals. However, the magnitude of these improvements varies with both precipitation intensity and the type of observations assimilated. A comparison among the three experimental configurations reveals that the temperature retrievals obtained from the GMWROnly and GWMRnMRL retrievals generally exhibit larger reductions in MB and $RMSE$ than those obtained from the MRLOnly retrievals. This behavior is physically reasonable given the characteristics of the observing systems. The GMWR includes multiple oxygen absorption channels that are directly sensitive to atmospheric temperature variations and therefore provide strong constraints on temperature retrievals. In contrast, the nitrogen Raman and water-vapor Raman channels of the MRL primarily contain information related to atmospheric moisture, resulting in a comparatively weaker impact on temperature retrieval accuracy. Consequently, retrievals incorporating GMWR observations are expected to outperform the MRLOnly retrievals with respect to temperature profile correction. Additionally, although the GWMRnMRL retrievals benefits from the complementary information provided by both observing systems, its temperature retrieval performance does not consistently exceed that of the GMWROnly retrievals. This finding suggests several possible explanations. First, while the adaptive observation weighting framework is effective at extracting information from individual observing systems, its capability to optimally balance information from multiple observation sources may still be limited, leaving room for further methodological improvements in multi-instrument retrieval applications. Second, the MRL configuration used in this study primarily provides water vapor-related information. It is therefore conceivable that incorporating advanced Raman lidar systems equipped with rotational Raman channels, which provide direct temperature observations in addition to water-vapor measurements, could enhance the temperature constraints available to the synergistic retrieval framework and thereby improve the performance of the GWMRnMRL retrievals. At present, however, these interpretations remain speculative and require additional experiments and observational studies for verification.

Table 2. Temperature Bias Reduction Rate

Evaluation Variable	Experiment Name	GMWROnly		GMRLOnly		GWMRnMRL	
	Test Name	Static	Adaptive	Static	Adaptive	Static	Adaptive

		Weighting	Weighting	Weighting	Weighting	Weighting	Weighting
MB	PI ∈ [10 mm, 20mm)	-0.412%	-0.575%	-0.396%	-0.561%	-0.394%	-0.558%
	PI ∈ [20 mm, 30mm)	-0.403%	-0.557%	-0.400%	-0.546%	-0.408%	-0.564%
	PI ∈ [30 mm, +∞)	-0.532%	-0.699%	-0.435%	-0.598%	-0.539%	-0.734%
	All Cases	-0.419%	-0.581%	-0.401%	-0.565%	-0.407%	-0.571%
$RMSE$	PI ∈ [10 mm, 20mm)	-0.356%	-0.746%	-0.348%	-0.752%	-0.317%	-0.696%
	PI ∈ [20 mm, 30mm)	-0.414%	-0.820%	-0.404%	-0.821%	-0.412%	-0.816%
	PI ∈ [30 mm, +∞)	-0.262%	-0.767%	-0.321%	-0.748%	-0.349%	-0.615%
	All Cases	-0.360%	-0.761%	-0.356%	-0.764%	-0.317%	-0.711%

Table 3 summarizes the MB and $RMSE$ reduction rates of the retrieved water vapor mass mixing ratio profiles for the GMWROnly, MRLOnly, and GWMRnMRL retrievals under different precipitation categories as well as for the complete heavy-precipitation dataset. Consistent with the findings presented in the preceding sections, the results further confirm that the adaptive observation weighting TCKF1D-Var framework achieves larger reductions in both MB and RMSE than the corresponding static observation weighting framework, demonstrating its superior capability for improving water vapor mass mixing ratio retrievals. From the perspective of MB reduction rates, the GWMRnMRL retrievals generally exhibits larger error reductions than either the GMWROnly or MRLOnly retrievals. This result indicates that the synergistic assimilation of GMWR and MRL observations provides additional constraints on atmospheric moisture profiles beyond those available from either observing system individually. However, the magnitude of the improvement obtained from the synergistic retrieval is substantially smaller than the sum of the improvements achieved by the two single-instrument experiments. Such behavior is expected because both observing systems contain overlapping information related to atmospheric water vapor concentration, resulting in a certain degree of information redundancy. At the same time, the non-additive nature of the improvement suggests that the adaptive observation weighting framework may not yet fully exploit the complementary information contained in multiple observation sources, leaving room for further methodological refinement. A different behavior is observed for the $RMSE$ reduction rates: the MRLOnly retrievals produces the largest $RMSE$ reductions among the three experimental configurations. Given that Raman lidar observations provide direct constraints on the vertical distribution of atmospheric moisture, this result highlights the strong contribution of MRL observations to water vapor mass mixing ratio retrieval accuracy. At the same time, the fact that the synergistic retrieval does not consistently outperform the MRLOnly experiment in terms of $RMSE$ reduction suggests that further improvements may be possible in the way multiple observation types are integrated within the adaptive observation weighting framework. In particular, future developments may focus on more effectively balancing redundant and complementary information from different observing systems during the retrieval process. A comparison between Tables 2 and 3 further reveals a consistent feature across all experiments. Regardless of whether single-instrument observations or synergistic GMWR–MRL observations are assimilated, both the adaptive and static observation weighting frameworks achieve substantially larger reductions in MB and $RMSE$ for water vapor mass mixing ratio than for temperature. This behavior is consistent with the observational characteristics of the instruments employed in this study and reinforces the conclusion that the primary benefit of the adaptive observation weighting framework lies in its enhanced ability to utilize humidity-related observational information for thermodynamic profile retrieval.

Table 3. Water Vapor Mass Mixing Ratio Bias Reduction Rate

Evaluation Variable	Experiment Name	GMWROnly		MRLOnly		GWMRnMRL	
	Test Name	Static Weighting	Adaptive Weighting	Static Weighting	Adaptive Weighting	Static Weighting	Adaptive Weighting
MB	PI ∈ [10 mm, 20mm)	-2.259%	-3.451%	-2.272%	-3.798%	-2.346%	-4.302%
	PI ∈ [20 mm, 30mm)	-2.065%	-3.118%	-2.225%	-3.661%	-2.317%	-4.057%
	PI ∈ [30 mm, +∞)	-2.167%	-3.681%	-2.154%	-3.024%	-2.224%	-3.674%
	All Cases	-2.221%	-3.406%	-2.248%	-3.745%	-2.327%	-4.205%
$RMSE$	PI ∈ [10 mm, 20mm)	-0.767%	-1.207%	-1.293%	-1.734%	-1.047%	-1.387%
	PI ∈ [20 mm, 30mm)	-0.745%	-1.259%	-1.527%	-1.998%	-1.217%	-1.606%
	PI ∈ [30 mm, +∞)	-0.879%	-1.151%	-1.053%	-1.511%	-1.166%	-0.977%
	All Cases	-0.786%	-1.220%	-1.315%	-1.762%	-1.106%	-1.400%

4.3.2 Relative observational contributions from different sensors

To investigate how the incorporation of MRL observations influences the channel weights assigned to GMWR observations within the adaptive observation weighting TCKF1D-Var framework, the differences between the channel weights diagnosed from the GMWR–MRL synergistic retrievals ($Weight_{GMWRnMRL}^{GMWR}$) and those obtained from the GMWROnly experiment ($Weight_{GMWROnly}$) were calculated. Specifically, the quantity $Weight_{GMWRnMRL}^{GMWR} - Weight_{GMWROnly}$ was used to quantify the impact of the synergistic retrieval on the weighting assigned to each GMWR channel. The resulting distributions are summarized in Figure 10 using boxplots for different precipitation categories.

Overall, the results indicate that the channels identified as the most stable and informative in the single-instrument experiments retain their dominant roles in the synergistic retrieval framework. In particular, the water-vapor channels at

22.235, 23.035, and 23.835 GHz and the oxygen absorption channels at 53.85, 54.94, and 56.66 GHz exhibit weight differences that remain centered near zero for most cases (Figure 10a), indicating that the introduction of MRL observations has only a limited impact on their diagnosed contributions. This behavior is consistent with the findings from Figure 4, where these channels were shown to possess consistently large weights and relatively small case-to-case variability. The persistence of these characteristics suggests that the information provided by these channels remains robust even when additional observational constraints are introduced. In contrast, the channels at 26.235, 51.25, and 52.28 GHz display a different behavior. For these channels, the median weight differences are generally positive, indicating that their relative contributions tend to increase when GMWR and MRL observations are assimilated simultaneously. However, the substantial separation between the median and mean values, together with the broad distributions and numerous outliers, reveals considerable case-to-case variability. Therefore, although these channels appear to benefit from the synergistic retrieval framework on average, their contributions remain strongly dependent on the specific atmospheric conditions associated with individual precipitation events. The precipitation-category analysis further supports this interpretation. The characteristics described above are particularly evident for the 10–20 mm cases (Figure 10b) and the ≥30 mm cases (Figure 10d), where the positive shifts in the median weights of the 26.235, 51.25, and 52.28 GHz channels are clearly visible. By comparison, the corresponding signals are less pronounced for the 20–30 mm category (Figure 10c), suggesting a weaker or less consistent response of these channels to the inclusion of MRL observations. Taken together, these results indicate that the synergistic retrieval framework primarily affects the channels that exhibited strong case dependence in the single-instrument experiments, while the most stable and information-rich channels remain largely unaffected by the introduction of additional observations.

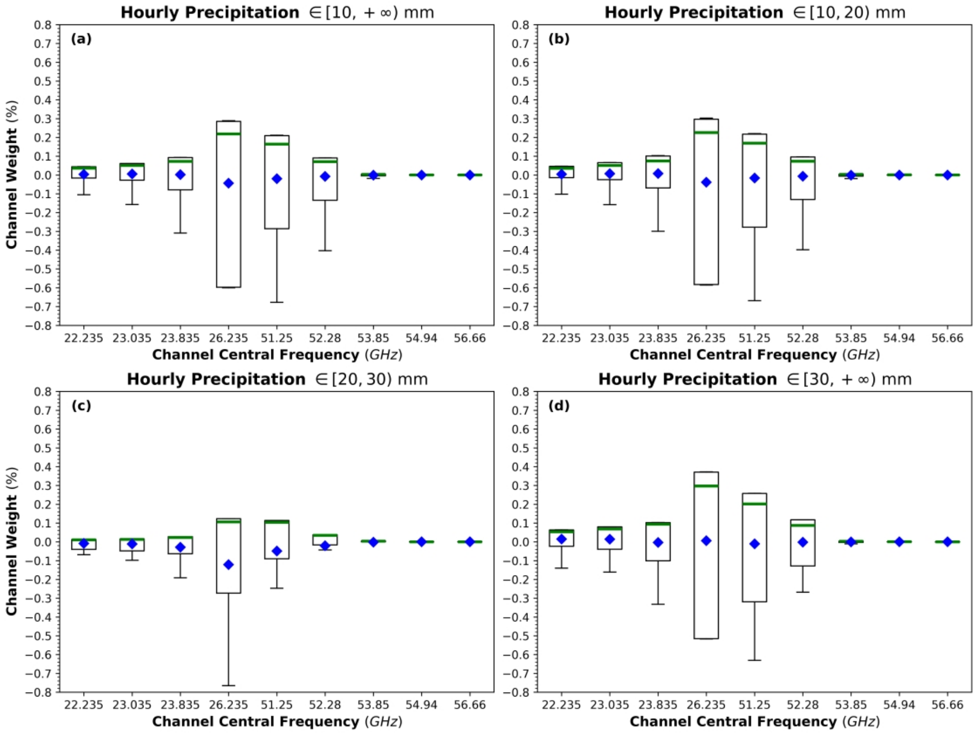

Figure 10. Boxplots of the differences in GMWR channel weights between the GWMRnMRL and GMWROnly experiments diagnosed by the adaptive observation weighting TCKF1D-Var framework. Results are shown for (a) all nocturnal heavy precipitation cases, (b) cases with hourly accumulated precipitation between 10 and 20 mm, (c) cases with hourly accumulated precipitation between 20 and 30 mm, and (d) cases with hourly accumulated precipitation exceeding 30 mm. The boxes represent the interquartile range (IQR), with the lower and upper edges corresponding to the first and third quartiles, respectively. The green horizontal lines indicate the median values, while the blue squares denote the mean values. Whiskers extend to 1.5 times the IQR, and red dots represent outliers beyond this range.

Using the same diagnostic approach as that employed for Figure 10, the impact of synergistic GMWR–MRL retrievals on the weights assigned to MRL observations was quantified by calculating the difference between the MRL weights diagnosed in the GWMRnMRL experiment ($Weight^{GMWR}_{GMWRnMRL}$) and those obtained from the MRLOnly experiment ($Weight_{GMWROnly}$). The resulting quantity, $Weight^{GMWR}_{GMWRnMRL} - Weight_{GMWROnly}$, provides a direct measure of how the inclusion of GMWR observations modifies the contribution of MRL observations within the adaptive observation weighting TCKF1D-Var framework. The statistical distributions of these weight differences are shown in Figure 11. For the complete dataset (Figure 11a), the influence of GMWR observations on the diagnosed MRL weights exhibits a clear height dependence. Below approximately 900 meters above ground level, the weight differences remain close to zero, indicating that the contribution of MRL observations in the adaptive weighting framework is largely unaffected by the addition of GMWR measurements. Between approximately 900 and 1800 meters, the weight differences become slightly positive, suggesting a modest enhancement of the contribution of MRL observations under synergistic retrieval conditions. In contrast, a noticeable reduction in MRL weights is observed between approximately 1800 and 3000 m, implying that part of the information previously attributed to MRL observations in the single-instrument retrievals is redistributed when GMWR observations are introduced. These features become even more pronounced in the 10–20 mm precipitation category (Figure 11b), which dominates the overall sample population. A different behavior emerges for the more intense precipitation categories. For cases with hourly accumulated precipitation between 20 and 30 mm and those exceeding 30 mm (Figure 11c and d), the distinct height-dependent patterns observed in Figure 11a and b become much less evident. This result suggests that the interaction between GMWR and MRL observations within the adaptive weighting framework is not constant but varies with precipitation intensity and the associated atmospheric conditions.

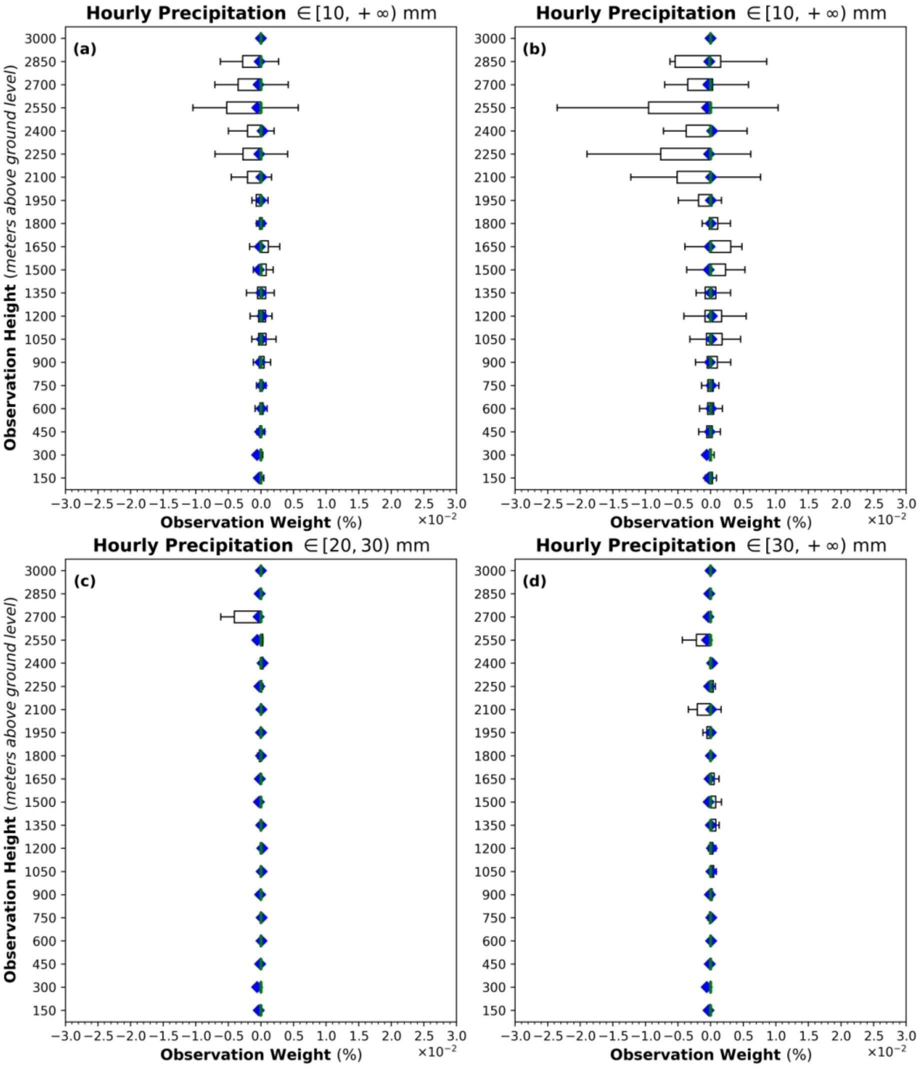

Figure 11. Same as Figure 10, but for the differences in MRL observation weights between the GWMRnMRL and MRLOnly experiments.

When Figures 10 and 11 are interpreted together with the retrieval statistics summarized in Table 3, several additional insights emerge. Table 3 indicates that the synergistic GWMRnMRL retrievals do not exhibit a simple additive improvement in water vapor mass mixing ratio retrieval accuracy. Although the synergistic retrieval generally achieves larger MB reduction rates than the corresponding single-instrument experiments, the magnitude of the improvement remains smaller than the sum of the individual contributions. Moreover, the $RMSE$ reduction rates do not consistently exceed those obtained from the MRLOnly experiment. The weight diagnostics provide a possible explanation for this behavior. As shown in Figure 10, the inclusion of MRL observations tends to increase the contribution of several GMWR channels, particularly those that exhibited strong case dependence in the single-instrument experiments. Conversely, Figure 11 shows that the contribution of MRL observations decreases at higher altitudes after GMWR observations are introduced. Together, these results suggest that the adaptive observation weighting framework actively redistributes observational influence between the two observing systems rather than simply combining their information content. Overall, the results confirm that the adaptive observation weighting TCKF1D-Var framework is capable of making more effective use of both single-instrument and synergistic observations than the corresponding static weighting framework. Nevertheless, the diagnosed redistribution of observational weights and the non-additive retrieval improvements indicate that opportunities remain for further methodological development. In particular, future work should focus on improving the exploitation of complementary information from multiple observing systems and on identifying strategies to better balance redundant and unique observational constraints within the retrieval framework.

5 Summary and concluding remarks

This study developed an adaptive observation weighting TCKF1D-Var retrieval framework and evaluated its performance for thermodynamic profile retrievals before nocturnal heavy-precipitation onset using ground-based microwave radiometer (GMWR) observations, Mie–Raman lidar (MRL) observations, and synergistic GMWR–MRL observations. A total of 107 nocturnal heavy-precipitation cases collected from 26 observational sites were used to assess the capability of the proposed framework and to compare its performance with that of a conventional static observation weighting TCKF1D-Var approach.

The results demonstrate that both the adaptive and static observation weighting frameworks are capable of utilizing GMWR and MRL observations to improve the prior thermodynamic profiles from ERA5 reanalysis dataset. However, the adaptive observation weighting strategy consistently achieves lower retrieval errors than the corresponding static weighting approach. The improvement is particularly evident for water vapor mass mixing ratio, whereas the impact on temperature retrievals is comparatively modest. For GMWROnly retrievals, the adaptive weighting framework reduces both the mean bias and root-mean-square error of the retrieved moisture profiles, with the largest improvements occurring between approximately 0.6 and 4.8 km above ground level. Similar behavior is observed for MRLOnly retrievals, where the adaptive weighting strategy

https://doi.org/10.5194/egusphere-2026-3341
Preprint. Discussion started: 9 July 2026

provides a more effective utilization of humidity-related observational information and leads to systematically improved moisture-profile retrievals.

The analysis of precipitation-intensity-dependent retrieval performance further indicates that the benefits of adaptive observation weighting are most robust for weak-to-moderate nocturnal heavy-precipitation events. Under the strongest precipitation conditions examined in this study, hourly accumulated precipitation exceeding 30 mm, the superiority of the adaptive weighting strategy becomes less apparent for GMWROnly retrievals, likely because increased observational uncertainties associated with heavy rainfall reduce the effectiveness of dynamically adjusting observation-error characteristics. Nevertheless, the adaptive weighting framework continues to provide measurable improvements for moisture retrievals based on MRL observations and synergistic multi-sensor retrievals. The diagnostic analysis of the adaptive weights provides additional insight into the behavior of the retrieval framework. For GMWR observations, six channels, including the 22.235, 23.035, 23.835, 53.85, 54.94, and 56.66 GHz channels, consistently receive large weights and exhibit relatively stable contributions across different precipitation conditions. In contrast, the 26.235, 51.25, and 52.28 GHz channels display stronger case-to-case variability, suggesting a more condition-dependent information content. For MRL observations, the adaptive weights generally increase with altitude, indicating that the framework assigns greater confidence to observations obtained above the lower troposphere. This behavior suggests that the adaptive weighting algorithm responds dynamically to the altitude-dependent characteristics of atmospheric moisture variability and observation uncertainty.

When GMWR and MRL observations are assimilated synergistically, the adaptive observation weighting framework continues to outperform the static weighting framework. The synergistic retrievals generally produce the smallest retrieval errors among all experiments, particularly for water vapor mass mixing ratio. However, the improvements obtained from the multi-sensor retrievals are not simply equal to the sum of the improvements achieved by the individual observing systems. Weight-diagnostic analyses reveal that the adaptive weighting framework actively redistributes observational influence between GMWR and MRL observations, increasing the contribution of some GMWR channels while reducing the contribution of MRL observations at certain altitudes. These findings indicate that the current framework is capable of exploiting both redundant and complementary information from multiple observing systems, but also suggest that the full potential of multi-sensor information fusion has not yet been realized.

Overall, the results demonstrate that the adaptive observation weighting TCKF1D-Var framework provides a practical and effective approach for improving thermodynamic profile retrievals under heavy-precipitation conditions. Compared with conventional static observation weighting, the proposed framework offers greater flexibility in balancing observational and background information and exhibits a consistently enhanced capability for retrieving atmospheric moisture profiles. At the same time, several limitations remain. The present study focused on a specific combination of GMWR and MRL observations and relied on a relatively limited number of intense precipitation cases. In addition, the physical mechanisms controlling the diagnosed adaptive weights were inferred indirectly from retrieval statistics and therefore require further investigation using dedicated observation-error diagnostics and information-content analyses. Future work will focus on extending the adaptive weighting methodology to additional observing systems, exploring more advanced strategies for multi-sensor information fusion, and evaluating its performance within coupled retrieval–data-assimilation frameworks. Such developments may further improve the utilization of complementary atmospheric observations and contribute to more accurate characterization of thermodynamic structures in severe weather environments.

Code and data availability

The exact version of the code and dataset used to produce the results presented in this study is archived on Zenodo (Zhang et al., 2026c; https://doi.org/10.5281/zenodo.20603287). All TCKF1D-Var retrieval products are stored in NetCDF format.

Author contributions

Tianmeng Chen prepared the observational data. Qi Zhang developed the TCKF1D-Var framework, performed the coding and data analysis, and drafted the manuscript. Tianmeng Chen revised the manuscript. Jianping Guo supervised the study as the principal investigator. Jianping Guo and Tianmeng Chen jointly secured major funding for this study, while Tianmeng Chen and Qi Zhang each secured additional independent funding from separate sources.

Competing interests

All authors delcare no competing interests.

Disclaimer

Copernicus Publications adds a standard disclaimer: “Copernicus Publications remains neutral with regard to jurisdictional claims made in the text, published maps, institutional affiliations, or any other geographical representation in this paper. While Copernicus Publications makes every effort to include appropriate place names, the final responsibility lies with the authors. Views expressed in the text are those of the authors and do not necessarily reflect the views of the publisher.” Please feel free to add disclaimer text at your choice, if applicable.

Acknowledgements

To be added upon acceptance.

Financial support

This manuscript was jointly supported by the Ministry of Science and Technology of China under grant 2024YFC3013001, the National Natural Science Foundation of China (NSFC) under grant 42325501, the Anhui Provincial Science and Technology Tackling Plan under grant 202523t06050001, and the Innovation and Development Special Project of the China Meteorological Administration under grant CXFZ2026J107.

References

Ahmed, F., Adames, Á. F., and Neelin, J. D.: Deep convective adjustment of temperature and moisture, J. Atmos. Sci., 77, 2163–2186, https://doi.org/10.1175/JAS-D-19-0227.1, 2020.

Askne, J. I. H. and Westwater, E. R.: A review of ground-based remote sensing of temperature and moisture by passive microwave radiometers, IEEE Trans. Geosci. Remote Sens., GE-24, 340–352, https://doi.org/10.1109/TGRS.1986.289591, 1986.

Barrera-Verdejo, M., Crewell, S., Löhnert, U., Orlandi, E., and Di Girolamo, P.: Ground-based lidar and microwave radiometry synergy for high vertical resolution absolute humidity profiling, Atmos. Meas. Tech., 9, 4013–4028, https://doi.org/10.5194/amt-9-4013-2016, 2016.

Behrendt, A., Pal, S., Aoshima, F., et al.: Observation of convection initiation processes with a suite of state-of-the-art research instruments during COPS IOP 8b, Q. J. R. Meteorol. Soc., 137, 81–100, https://doi.org/10.1002/qj.758, 2011

Behrendt, A., Pal, S., Aoshima, F., et al.: Observation of convection initiation processes with a suite of state-of-the-art research instruments during COPS IOP 8b, Q. J. R. Meteorol. Soc., 137, 81–100, https://doi.org/10.1002/qj.758, 2011.

Böck, T., Löffler, M., Marke, T., Pospichal, B., Knist, C., and Löhnert, U.: Instrument uncertainties of network-suitable ground-based microwave radiometers: overview, quantification, and mitigation strategies, Atmos. Meas. Tech., 18, 6251–6270, https://doi.org/10.5194/amt-18-6251-2025, 2025.

Cao, X., Guo, Q., Luo, H., Wang, J., Yang, R., Xiao, D., Liu, Y., Sun, Z., Liu, S., Chen, S., Huang, A., Jianping, G., and Zhang, P.: Development and application of the Ascent-Drift-Descent Radiosonde System (ADDRS), Atmos. Meas. Tech., 19, 3231–3251, https://doi.org/10.5194/amt-19-3231-2026, 2026.

Chen, Y., Wang, X., Huang, L., and Luo, Y.: Spatial and temporal characteristics of abrupt heavy rainfall events over Southwest China during 1981–2017, Int. J. Climatol., 41, 3286–3299, https://doi.org/10.1002/joc.7019, 2021.

Cimini, D., Nelson, M., Güldner, J., and Ware, R.: Forecast indices from a ground-based microwave radiometer for operational meteorology, Atmos. Meas. Tech., 8, 315–333, https://doi.org/10.5194/amt-8-315-2015, 2015.

Di Girolamo, P., Cacciani, M., Summa, D., et al.: Characterisation of boundary layer turbulent processes by Raman lidar BASIL, Atmos. Chem. Phys., 17, 745–767, https://doi.org/10.5194/acp-17-745-2017 , 2017.

Esri, DeLorme, HERE, TomTom, Intermap, increment P Corp., GEBCO, USGS, FAO, NPS, NRCAN, GeoBase, IGN, Kadaster NL, Ordnance Survey, Esri Japan, METI, Esri China (Hong Kong), swisstopo, and MapmyIndia: World Imagery, available at: https://www.arcgis.com/home/item.html?id=10df2279f9684e4a9f6a7f08febac2a9 (last access: 14 Apr. 2026), 2025.

Filioglou, M., Nikandrova, A., Niemelä, S., et al.: Profiling water vapor mixing ratios in Finland by Raman lidar, Atmos. Meas. Tech., 10, 4303–4316, https://doi.org/10.5194/amt-10-4303-2017, 2017.

Foth, A., Baars, H., Di Girolamo, P., and Pospichal, B.: Water vapour profiles from Raman lidar automatically calibrated by microwave radiometer data during HOPE, Atmos. Chem. Phys., 15, 7753–7763, https://doi.org/10.5194/acp-15-7753-2015, 2015.

Gambacorta, A., et al.: Improved planetary boundary layer sounding using hyperspectral microwave and lidar data fusion, IEEE Trans. Geosci. Remote Sens., 63, 1–23, https://doi.org/10.1109/TGRS.2025.3630972, 2025.

Gao, Z., Li, L., Zhao, C., Gao, G., Jiang, R., Yang, H., Liu, S., and Lu, P.: Impacts of distinct synoptic patterns on fine-scale precipitation characteristics in complex terrain of Southwestern China, Int. J. Climatol., e70315, https://doi.org/10.1002/joc.70315, 2026.

Gerber, D., Balin, I., Feist, D. G., Kämpfer, N., Simeonov, V., Calpini, B., and van den Bergh, H.: Ground-based water vapour soundings by microwave radiometry and Raman lidar on Jungfraujoch (Swiss Alps), Atmos. Chem. Phys., 4, 2171–2179, https://doi.org/10.5194/acp-4-2171-2004, 2004.

Gerber, F. and Furrer, R.: optimParallel: An R package providing a parallel version of the L-BFGS-B optimization method, R J., https://doi.org/10.32614/RJ-2019-030, 2019.

Güldner, J., and D. Spänkuch: Remote Sensing of the Thermodynamic State of the Atmospheric Boundary Layer by Ground-Based Microwave Radiometry. J. Atmos. Oceanic Technol., 18, 925–933, https://doi.org/10.1175/1520-0426(2001)018<0925:RSOTTS>2.0.CO;2, 2001.

Han, Y., J. B.Snider, E. R.Westwater, S. H.Melfi, and R. A.Ferrare: Observations of water vapor by ground-based microwave radiometers and Raman lidar, J. Geophys. Res., 99(D9), 18695–18702, https://doi.org/10.1029/94JD01487, 1994.

Hersbach, H., Bell, B., Berrisford, P., et al.: The ERA5 global reanalysis, Q. J. R. Meteorol. Soc., 146, 1999–2049, https://doi.org/10.1002/qj.3803, 2020.

Hewison, T. J.: 1D-VAR retrieval of temperature and humidity profiles from a ground-based microwave radiometer, IEEE Trans. Geosci. Remote Sens., 45, 2163–2168, https://doi.org/10.1109/TGRS.2007.898091, 2007.

Ji, C., Jin, Q., Li, F., Liu, Y., Wang, Z., Mao, J., Ren, X., Xiang, Y., Jian, W., Chen, Z., and Zhao, P.: A new method to retrieve relative humidity profiles from a synergy of Raman lidar, microwave radiometer, and satellite, Atmos. Meas. Tech., 18, 3179–3191, https://doi.org/10.5194/amt-18-3179-2025, 2025.

Kirshbaum, D. J., Adler, B., Kalthoff, N., Barthlott, C., and Serafin, S.: Moist orographic convection: Physical mechanisms and links to surface-exchange processes, Atmosphere, 9, 80, https://doi.org/10.3390/atmos9030080, 2018.

Lange, D., Behrendt, A., and Wulfmeyer, V.: Compact operational tropospheric Raman lidar, Geophys. Res. Lett., 46, 14844–14853, https://doi.org/10.1029/2019GL085774, 2019.

Lange, D., Behrendt, A., Senff, C., et al.: Water–vapor budget investigation using ground-based lidar, Bull. Atmos. Sci. Technol., 6, 24, https://doi.org/10.1007/s42865-025-00110-4, 2025.

Luo, Y. L., Sun, J. S., Li, Y., et al.: Science and prediction of heavy rainfall over China: Research progress since the reform and opening-up of new China, J. Meteorol. Res., 34, 427–459, https://doi.org/10.1007/s13351-020-0006-x, 2020.

Löhnert, U. and Maier, O.: Operational profiling of temperature using ground-based microwave radiometry at Payerne: prospects and challenges, Atmos. Meas. Tech., 5, 1121–1134, https://doi.org/10.5194/amt-5-1121-2012, 2012.

Löhnert, U., Necker, T., Schnitt, S., Toporov, M., Andersson, E., August, T., Collard, A., Diefenbach, T., Eingrüber, N., Erraji, H., Fowler, A., Franke, P., Franzoni, S., Lange, A. C., Lessig, C., Nikfal, A., Raabe, N., Scheck, L., Schewior, K., Weber, H., and Žagar, N.: How to Design the Future Earth Observation System? Bulletin of the American Meteorological Society (published online ahead of print 2026), BAMS-D-26-0150.1, BAMS-D-26-0150.1, https://doi.org/10.1175/BAMS-D-26-0150.1, 2026.

Löhnert, U., S. Crewell, and C. Simmer: An Integrated Approach toward Retrieving Physically Consistent Profiles of Temperature, Humidity, and Cloud Liquid Water. J. Appl. Meteor. Climatol., 43, 1295–1307, https://doi.org/10.1175/1520-0450(2004)043<1295:AIATRP>2.0.CO;2, 2004.

Ma, W., Ma, W., Xie, Z. et al.: Unique atmospheric boundary layer structures driven by lake effects. Commun Earth Environ 7, 221, https://doi.org/10.1038/s43247-026-03234-3, 2026.

Meunier, V., D. D. Turner, and P. Kollias: On the Challenges of Tomography Retrievals of a 2D Water Vapor Field Using Ground-Based Microwave Radiometers: An Observation System Simulation Experiment. J. Atmos. Oceanic Technol., 32, 116–130, https://doi.org/10.1175/JTECH-D-13-00194.1, 2015.

Richardson, M. T., Kahn, B. H., and Kalmus, P. M.: Mesoscale air motion and thermodynamics predict heavy hourly U.S. precipitation, Commun. Earth Environ., 5, 472, https://doi.org/10.1038/s43247-024-01614-1, 2024.

Shao, N., Wang, Q., Bu, Z., Yin, Z., Dai, Y., Chen, Y., and Wang, X.: China aerosol Raman lidar network (CARLNET), Remote Sens., 17, 414, https://doi.org/10.3390/rs17030414, 2025.

Sun, X., Yang, Z., and Niyogi, D.: Diurnal urban rainfall anomalies across different landscapes, Sci. Adv., 11, eads5046, https://doi.org/10.1126/sciadv.ads5046, 2025.

Temimi, M., Fonseca, R. M., Nelli, N. R., Valappil, V. K., Weston, M. J., Thota, M. S., Wehbe, Y., and Yousef, L.: On the analysis of ground-based microwave radiometer data during fog conditions, Atmos. Res., 231, 104652, https://doi.org/10.1016/j.atmosres.2019.104652, 2020.

Vaughan, G., Wareing, D. P., Thomas, L., and Mitev, V.: Humidity measurements in the free troposphere using Raman backscatter, Q. J. R. Meteorol. Soc., 114, 1471–1484, https://doi.org/10.1002/qj.49711448406, 1988.

Wandinger, U.: Raman lidar, in: Lidar, Springer, New York, https://doi.org/10.1007/0-387-25101-4_9, 2005.

Whiteman, D. N., Rush, K., Rabenhorst, S., et al.: Airborne and ground-based measurements using a high-performance Raman lidar, J. Atmos. Ocean. Technol., 27, 1781–1801, https://doi.org/10.1175/2010JTECHA1391.1, 2010.

Wulfmeyer, V., Behrendt, A., Kottmeier, C., et al.: The convective and orographically induced precipitation study (COPS): Scientific strategy and highlights, Q. J. R. Meteorol. Soc., 137, 3–30, https://doi.org/10.1002/qj.752, 2011.

Wulfmeyer, V., Behrendt, A., Kottmeier, C., et al.: The convective and orographically induced precipitation study (COPS): Scientific strategy and highlights, Q. J. R. Meteorol. Soc., 137, 3–30, https://doi.org/10.1002/qj.752, 2011.

Wulfmeyer, V., Hardesty, R. M., Turner, D. D., Behrendt, A., Cadeddu, M. P., Di Girolamo, P., Schlüssel, P., Van Baelen, J., and Zus, F.: A review of the remote sensing of lower tropospheric thermodynamic profiles and its indispensable role for the understanding and the simulation of water and energy cycles, Rev. Geophys., 53, 819–895, https://doi.org/10.1002/2014RG000476, 2015.

Yan, X., Liang, C., Jiang, Y., Luo, N., Zang, Z., and Li, Z.: A deep learning approach to improve the retrieval of temperature and humidity profiles from a ground-based microwave radiometer, IEEE Trans. Geosci. Remote Sens., 58, 8427–8437, https://doi.org/10.1109/TGRS.2020.2987896, 2020.

Zhang, P., Li, R., Zhao, K., Wang, D., Wang, J., Lei, Y., Xia, X., Xian, D., Chen, Y., Wu, L., Zhao, P., Guo, Q., Yang, R., Li, C., Yan, P., Liu, C., Wang, X., Gui, H., Liu, L., Guan, M., Huang, H., He, J., Liu, L., Wang, B., Sun, Y., Wang, Y., Huang, Y., Hu, W., Li, B., Wang, Z., Ma, Y., Liu, J., and Fu, Y.: Development of an integrated meteorological observation system in China, Acta Meteorol. Sin., 83, 729–760, https://doi.org/10.11676/qxxb2025.20240193, 2025.

Zhang, Q., Chen, T., and Guo, J.: Extended TCKF1D-Var framework for Mie–Raman Lidar Water Vapor Profiling in the Nocturnal Boundary Layer: Insights into Pre-precipitation Moisture Evolution, EGUsphere [preprint], https://doi.org/10.5194/egusphere-2026-2184, 2026b.

Zhang, Q., Chen, T., and Guo, J.: Ground-Based Multi-Sensor Thermodynamic Retrievals Prior to Nocturnal Heavy Precipitation over China [Data set]. Zenodo. https://doi.org/10.5281/zenodo.20603287, 2026c.

Zhang, Q., Chen, T., Guo, J., Wu, Y., Deng, B., and Yan, J.: Retrieving atmospheric thermodynamic and hydrometeor profiles using a thermodynamic-constrained Kalman filter 1D-Var framework based on ground-based microwave radiometer, Geosci. Model Dev., 19, 505–522, https://doi.org/10.5194/gmd-19-505-2026, 2026a.

Zhang, W., Guo, J., Miao, Y., Liu, H., Song, Y., Fang, Z., He, J., Lou, M., Yan, Y., Li, Y., and Zhai, P: On the Summertime Planetary Boundary Layer with Different Thermodynamic Stability in China: A Radiosonde Perspective. Journal of Climate, 31(4), 1451-1465. https://doi.org/10.1175/JCLI-D-17-0231.1, 2018.